J. Fluid Mech. (1986), *vol.* 173, *pp.* 159–189
Printed in Great Britain

Viscous starting jets

By BRIAN J. CANTWELL
Stanford University, Stanford, CA 94305, USA

(Received 26 March 1986)

This paper is concerned with the transient motion produced when a viscous incompressible fluid is forced from an initial state of rest. The applied force is time dependent in the form of an impulse, step and ramp function applied at a point and along a line. These cases have been chosen because they form a logical progression for investigating the connection between the flow Reynolds number and the sequence of events leading to the creation of a starting vortex. Much of the structure of the starting process can be revealed through a study of boundary conditions, integrals of the motion and the invariance properties of the governing equations prior to the consideration of a particular solution. The method used to bring out the flow structure is applicable to flows that can be treated as self-similar over some interval in time. The equations for unsteady particle paths are written in terms of similarity variables and then analysed as a quasi-autonomous system with the, usually time-dependent, Reynolds number treated as a parameter. The structure of the flow is examined by finding and classifying critical points in the phase portrait of this system. Bifurcations in the phase portrait are found to occur at specific values of the Reynolds number of the flow in question. When exact solutions of the Stokes equations for the low-Reynolds-number limit are examined they are found to contain two critical Reynolds numbers and three distinct states of motion which culminate in the onset of a vortex roll-up. An interesting feature of the Stokes solutions for planar unsteady jets is that they are uniformly valid over $0 < r < \infty$.

1. Introduction

A phase-plane approach was used by Oswatitsch (1958) and Lighthill (1963) to describe the topology of flow patterns near a solid wall. More recently Perry and his co-workers (Perry & Fairlie 1974; Perry, Lim & Chong 1980; Perry & Chong 1987, a review) have made extensive use of critical-point theory to describe complex flow patterns in steady and unsteady three-dimensional flows. In studies of aerodynamic flows the method has been widely used to interpret surface skin-friction patterns visualized using oil-flow or china-clay techniques (see the review by Tobak & Peake 1982). In all of this work the flow patterns are described in a phase space corresponding to physical coordinates.

In the present work the flow patterns in viscous jets are described in a phase space of similarity coordinates. This approach was used by Cantwell, Coles & Dimotakis (1978) to describe the self-similar flow in the plane of symmetry of a turbulent spot. Experimental data were collapsed onto $(x/t, y/t)$ coordinates and the phase portrait of particle paths was used to determine the rate at which fluid was entrained into various regions on the centreline of the spot. Glezer (1981) used $(x/t^{\frac{1}{4}}, y/t^{\frac{1}{4}})$ coordinates to freeze the large-scale structure of a turbulent vortex ring. In both of these cases, non-self-similar motions following a viscous timescale were averaged out through the use of the large-eddy timescale for assigning phase information to the velocity data.

Turner (1964) used a Hill's spherical vortex in $(x/t, y/t)$ coordinates to model entrainment in a buoyant thermal rising at constant velocity. Recently Turner's model has been modified by Griffiths (1986) to include viscous effects. A Stokes flow solution in $(r/t^{\frac{1}{2}}, \theta)$ coordinates is used to describe particle paths in and about a region of constant total buoyancy rising at a velocity proportional to $1/t^{\frac{1}{2}}$. The new model is used to explain laboratory observations of the distortion of buoyant dyed fluid blobs for low, intermediate and high values of the Rayleigh number.

Critical Reynolds numbers in the starting process of a round jet were determined by Cantwell (1981*a*) using a Stokes flow approximation in $(r/t^{\frac{1}{2}}, \theta)$ coordinates. It was shown that transition in this constant-Reynolds-number flow is in the nature of a sequence of bifurcations in the phase portrait of particle paths which occur as the Reynolds number is increased. The process is reminiscent of transition in Couette flow studied by G. I. Taylor in 1923 except that the basic flow is time dependent and set in an infinite domain. A numerical calculation of the round jet was carried out up to a Reynolds number of 30 by Allen (1984). The critical Reynolds numbers of the full nonlinear problem were shown to be lower than those deduced from the Stokes approximation although the basic topology of the flow was the same. The technique was extended by Cantwell & Allen (1984) to the cases of the vortex ring produced by an impulsive force and a ramp jet produced by a force which increases linearly with time. In these cases the particle-path equations in similarity coordinates are not autonomous. Nevertheless the instantaneous phase portrait still contains useful information about the flow. It provides a physical picture of the tendency for the flow to roll or stretch a fluid line. Critical Reynolds numbers (dimensionless times) at which changes in flow topology occur can be identified and conclusions can be drawn about the mechanics of the starting process. In addition the method provides a basis for comparison of various flows under different conditions of forcing. Changes in flow structure with Reynolds number and trends with various types of forcing which may not be apparent when one views the flow in terms of the velocity or vorticity field often become evident when the flow is viewed in terms of its phase portrait.

2. The impulse integral

In this section the momentum equation is integrated over a spherical control volume which contains the vorticity-bearing region. This leads to a relationship between the force applied at the origin of the flow, the far-field distribution of pressure and the total hydrodynamic impulse. Figure 1 depicts the physical situation we wish to treat. A system of forces $\boldsymbol{F}(\boldsymbol{x}, t)$ (force per unit volume) acts on a viscous fluid inside a volume V with surface normal vector $\boldsymbol{n}\mathrm{d}S$. The force distribution and its associated vorticity distribution are assumed to occupy a finite region within V. The fluid is incompressible and extends to infinity,

$$\nabla \cdot \boldsymbol{u} = 0. \tag{2.1}$$

The vorticity is defined by

$$\nabla \times \boldsymbol{u} = \boldsymbol{\omega}. \tag{2.2}$$

Since there are no volume sources in V the velocity can be expressed purely as the curl of a vector potential $\boldsymbol{A}$:

$$\boldsymbol{u} = \nabla \times \boldsymbol{A}. \tag{2.3}$$

The divergence of $\boldsymbol{A}$ is arbitrary. The convenient choice of a Coulomb gauge $\nabla \cdot \boldsymbol{A} = 0$ leads, with the aid of a vector identity, to the vector Poisson equation

$$\nabla^2 \boldsymbol{A} = -\boldsymbol{\omega}, \tag{2.4}$$

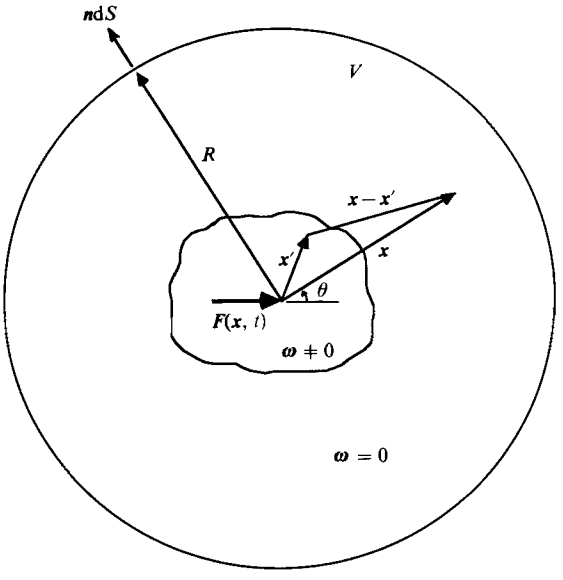

FIGURE 1. Sketch of the flow with applied force.

the solution of which is
$$\boldsymbol{A}(\boldsymbol{x},t)=\frac{1}{4\pi}\int_V\frac{\boldsymbol{\omega}(\boldsymbol{x}',t)}{|\boldsymbol{x}-\boldsymbol{x}'|}\,\mathrm{d}\boldsymbol{x}', \tag{2.5}$$

where $\mathrm{d}\boldsymbol{x}'$ is a volume element in V. We want to find an expression for the volume-integrated momentum divided by the density given by

$$\boldsymbol{H}(t)=\int_V\boldsymbol{u}(\boldsymbol{x},t)\,\mathrm{d}\boldsymbol{x}, \tag{2.6}$$

which we can write as a surface integral of the vector potential

$$\boldsymbol{H}(t)=\int_S\boldsymbol{n}\times\boldsymbol{A}(\boldsymbol{x},t)\,\mathrm{d}S=R^2\int_S\left(\frac{\boldsymbol{x}}{R}\right)\times\boldsymbol{A}(\boldsymbol{x},t)\,\mathrm{d}\Omega, \tag{2.7}$$

where $\boldsymbol{n}=\boldsymbol{x}/R=\boldsymbol{i}(\sin\theta\cos\phi)+\boldsymbol{j}(\sin\theta\sin\phi)+\boldsymbol{k}(\cos\theta)$ and $\mathrm{d}\Omega$ is an infinitesimal solid angle $\mathrm{d}\Omega=\sin\theta\,\mathrm{d}\theta\,\mathrm{d}\phi$. Substituting the expression for $\boldsymbol{A}$ from (2.5) into (2.7), exchanging the order of integration and making use of the fact that $\int_S\boldsymbol{x}/|\boldsymbol{x}-\boldsymbol{x}'|\,\mathrm{d}\Omega=(\frac{4}{3}\pi)\,(\boldsymbol{x}/R)$ leads to

$$\boldsymbol{H}(t)=\tfrac{2}{3}\boldsymbol{I}(t), \tag{2.8}$$

where
$$\boldsymbol{I}(t)=\frac{1}{2}\int_V\boldsymbol{x}\times\boldsymbol{\omega}(\boldsymbol{x},t)\,\mathrm{d}\boldsymbol{x} \tag{2.9}$$

is called the impulse of the vorticity distribution (Lamb 1932). In two dimensions

$$\int_V\boldsymbol{u}(\boldsymbol{x},t)\,\mathrm{d}\boldsymbol{x}=\frac{1}{2}\int_V\boldsymbol{x}\omega_z(\boldsymbol{x},t)\,\mathrm{d}\boldsymbol{x}, \tag{2.10}$$

where the integration is confined to the upper half-plane. The integral of the momentum is fully converged as long as the sphere contains all of the vorticity. Potential-flow motions beyond the vortical region do not contribute to the total momentum.

2.1. *Far-field vector potential and pressure*

In order to actually evaluate the impulse integral (2.9) we need to carry out an integral momentum balance over V. Integrating the momentum equation and making use of the divergence theorem gives

$$\frac{\mathrm{d}\boldsymbol{H}}{\mathrm{d}t}+\int_S \left\{\boldsymbol{uu}+\frac{p}{\rho}\boldsymbol{I}-\nu\boldsymbol{\nabla u}\right\}\cdot\boldsymbol{n}\,\mathrm{d}S=\int_V \frac{\boldsymbol{F}(\boldsymbol{x},t)}{\rho}\,\mathrm{d}\boldsymbol{x}. \tag{2.11}$$

At large values of r the vector potential may be approximated by the first few terms of a multipole expansion

$$\boldsymbol{A}=\frac{\boldsymbol{q}}{4\pi r}+\frac{\boldsymbol{Q}\cdot\boldsymbol{x}}{4\pi r^3}+O\left(\frac{1}{r^3}\right), \tag{2.12}$$

where

$$\boldsymbol{q}=-\int_V \boldsymbol{\omega}(\boldsymbol{x}',t)\,\mathrm{d}\boldsymbol{x}'; \quad \boldsymbol{Q}=-\int_V \boldsymbol{\omega}(\boldsymbol{x}',t)\,\boldsymbol{x}'\,\mathrm{d}\boldsymbol{x}'. \tag{2.13}$$

The fact that $\boldsymbol{\omega}$ is divergence free and localized and $\boldsymbol{F}(\boldsymbol{x},t)$ applies no net moment to the fluid implies that $\boldsymbol{q}=0$. The numerator of the second term in (2.12) can be written

$$\boldsymbol{Q}\cdot\boldsymbol{x}=-\boldsymbol{x}\times\left\{\frac{1}{2}\int_V \boldsymbol{x}'\times\boldsymbol{\omega}(\boldsymbol{x}',t)\,\mathrm{d}\boldsymbol{x}'\right\}. \tag{2.14}$$

Thus at large r the vector potential to lowest order is

$$\boldsymbol{A}=\frac{1}{4\pi}\frac{\boldsymbol{I}(t)\times\boldsymbol{x}}{r^3}+O\left(\frac{1}{r^3}\right). \tag{2.15}$$

The results given in (2.8), (2.9) and (2.15) all follow directly by analogy with classical results from magnetostatics. The velocity $\boldsymbol{u}$ is analogous to the magnetic field, the vorticity $\boldsymbol{\omega}/4\pi$ is analogous to the current density; see for example Jackson (1977). Using (2.15) we can estimate the surface integrals of the nonlinear and viscous terms in (2.11) as

$$\lim_{R\to\infty}\int_S (\boldsymbol{uu})\cdot\boldsymbol{n}\,\mathrm{d}S\sim\frac{1}{R^4}; \quad \lim_{R\to\infty}\int_S (\boldsymbol{\nabla u})\cdot\boldsymbol{n}\,\mathrm{d}S\sim\frac{1}{R^2}. \tag{2.16}$$

Thus as $R\to\infty$

$$\frac{\mathrm{d}\boldsymbol{H}}{\mathrm{d}t}+\int_S \left(\frac{p}{\rho}\right)\boldsymbol{n}\,\mathrm{d}S=\int_V \frac{\boldsymbol{F}(\boldsymbol{x},t)}{\rho}\,\mathrm{d}\boldsymbol{x}. \tag{2.17}$$

The momentum equation at large r is

$$\frac{\partial\boldsymbol{u}}{\partial t}+\frac{1}{\rho}\boldsymbol{\nabla}p=0. \tag{2.18}$$

We can use (2.18) to determine an expression for the far-field pressure. Using (2.15) for the vector potential and the fact that $\boldsymbol{\nabla}\cdot(\boldsymbol{x}/r^3)=\boldsymbol{\nabla}\times(\boldsymbol{x}/r^3)=0$ we can write the velocity as the gradient of a scalar. At large r

$$\boldsymbol{u}=-\frac{1}{4\pi}\boldsymbol{\nabla}\left\{\frac{\boldsymbol{I}\cdot\boldsymbol{x}}{r^3}\right\}. \tag{2.19}$$

Substituting (2.19) into (2.18) and solving we have, to within an additive function of time,

$$\frac{p}{\rho}=\frac{1}{4\pi}\left(\frac{\mathrm{d}\boldsymbol{I}}{\mathrm{d}t}\right)\cdot\frac{\boldsymbol{x}}{r^3}. \tag{2.20}$$

The surface integral of the pressure in (2.17) may now be evaluated as

$$\int_S \left(\frac{p}{\rho}\right) \boldsymbol{n}\, \mathrm{d}S = \frac{1}{3}\frac{\mathrm{d}\boldsymbol{I}}{\mathrm{d}t}, \tag{2.21}$$

where the integral is over the surface of a sphere at $R \to \infty$. Substituting (2.21) and (2.8) into (2.17) and integrating over time gives

$$\boldsymbol{I}(t) = \int_0^t \int_V \frac{\boldsymbol{F}(\boldsymbol{x}, t)}{\rho}\, \mathrm{d}\boldsymbol{x}\, \mathrm{d}t. \tag{2.22}$$

The integral $\boldsymbol{I}(t)$ is the total impulse applied to the force distribution since the onset of the motion. According to (2.8) two-thirds of the applied impulse ends up in the momentum of the fluid, the remaining one-third is removed by the pressure field at infinity which opposes the motion. In two dimensions

$$\int_S \left(\frac{p}{\rho}\right) \boldsymbol{n}\, \mathrm{d}S = \frac{1}{2}\frac{\mathrm{d}\boldsymbol{I}}{\mathrm{d}t}. \tag{2.23}$$

In the two-dimensional case where the vorticity extends to $z \to \pm\infty$, the monopole term in the expansion of the vector potential (stream function) is assumed to be zero so that there is no net circulation in the flow.

2.2. *Governing parameters*

For the three-dimensional case we shall choose $\boldsymbol{F}(\boldsymbol{x}, t)/\rho$ to be of the form

$$\frac{\boldsymbol{F}(\boldsymbol{x}, t)}{\rho} = (0, 0, Mf(t)\,\delta(x)\,\delta(y)\,\delta(z)), \tag{2.24}$$

where the force is directed along the z-axis in a system of spherical polar coordinates. For the two-dimensional cases

$$\frac{\boldsymbol{F}(\boldsymbol{x}, t)}{\rho} = (Mf(t)\,\delta(x)\,\delta(y), 0), \tag{2.25}$$

where the force is directed along the x-axis in a system of cylindrical polar coordinates. The quantity M is an amplitude parameter for the force. The dimensions of $\boldsymbol{F}/\rho$ are LT^{-2}. Thus

$$\text{units of } M = L^m T^{-n}, \tag{2.26}$$

where

$$\left.\begin{aligned} m = 4;&\quad \text{three-dimensional (point) force,}\\ m = 3;&\quad \text{two-dimensional (line) force,}\end{aligned}\right\} \tag{2.27}$$

and for the three cases of an impulse, step and ramp forcing

$$\left.\begin{aligned} n = 1;&\quad f(t) = \delta(t),\\ n = 2;&\quad f(t) = h(t),\\ n = 3;&\quad f(t) = th(t),\end{aligned}\right\} \tag{2.28}$$

where $h(t)$ is the Heaviside function and $\delta(t)$ is the delta function. The corresponding impulse integrals are

$$\left.\begin{aligned} \boldsymbol{I}(t) &= \left(0, 0, \frac{Mt^{mk-1}}{(n-1)}\right);\quad \text{point force,}\\ \boldsymbol{I}(t) &= \left(\frac{Mt^{mk-1}}{(n-1)}, 0\right);\quad \text{line force,}\end{aligned}\right\} \tag{2.29}$$

where $$k = n/m, \tag{2.30}$$

and it is understood that when $n = 1$ the term $(n-1)$ is set to 1. In the next section we shall use the scalar impulse $I(t) = Mt^{mk-1}/(n-1)$ and the unit parameters m and n to generate similarity forms of the governing equations.

3. Invariant groups and similarity forms

In this section general similarity variables and functional forms are constructed using the invariance of the governing equations, boundary conditions and impulse integral under a two-parameter group of stretching transformations. The Stokes, Navier–Stokes and Euler equations are considered and the results are combined to identify an appropriate time-dependent Reynolds number for each flow case.

The nature of the forcing and, in effect, the units of M have a pervading influence on the evolution of length and velocity scales in the flow. To the extent that the force distribution has no lengthscale of its own, M and ν are the only parameters which appear in the problem. This fact, combined with the simple geometry of an unbounded flow at infinity, suggests the possible existence of a similarity solution.

3.1. *The Stokes equations*

The Stokes equations

$$\left.\begin{aligned} \frac{\partial u_i}{\partial x_i} &= 0, \\ \frac{\partial u_i}{\partial t} + \frac{1}{\rho}\frac{\partial p}{\partial x_i} - \nu\frac{\partial^2 u_i}{\partial x_j\,\mathrm{d}x_j} &= 0, \end{aligned}\right\} \tag{3.1}$$

are invariant under the two-parameter group of stretching transformations

$$\left.\begin{aligned} x_i &= \mathrm{e}^{a}\,\hat{x}_i, \\ t &= \mathrm{e}^{2a}\,\hat{t}, \\ u_i &= \mathrm{e}^{ab}\,\hat{u}_i, \\ \frac{p}{\rho} &= \mathrm{e}^{a(b-1)}\,\frac{\hat{p}}{\rho}, \end{aligned}\right\} \tag{3.2}$$

where a and b are arbitrary. Substitution of (3.2) into (3.1) generates a set of equations identical with (3.1) but in terms of new variables, thus confirming the invariance. When we require further that the impulse integrals (2.29) be invariant under (3.2) then, in three dimensions,

$$\int u_z\,\mathrm{d}^3x = \frac{2}{3}\frac{Mt^{4k-1}}{(n-1)}, \tag{3.3}$$

which, when transformed according to (3.2), becomes

$$\mathrm{e}^{a(b+3)}\int \hat{u}_z\,\mathrm{d}^3\hat{x} = \mathrm{e}^{a(8k-2)}\,\frac{2}{3}\frac{Mt^{4k-1}}{(n-1)}. \tag{3.4}$$

The two-dimensional impulse integral

$$\int u_x\,\mathrm{d}^2x = \frac{1}{2}\frac{Mt^{3k-1}}{(n-1)} \tag{3.5}$$

becomes

$$e^{a(b+2)} \int \hat{u}_x \, d^2\hat{x} = e^{a(6k-2)} \frac{1}{2} \frac{M t^{3k-1}}{(n-1)}. \tag{3.6}$$

For invariance we require in both cases

$$b = 2mk - (m+1). \tag{3.7}$$

The nature of the forcing determines the time dependence of the impulse integral and the units of M. The unit parameters m and n in turn determine the value of b which leaves both the equations and impulse-integral invariant under the group (3.2). The parameter a remains arbitrary. The invariance of the overall problem under (3.2) confirms the existence of similarity solutions.

Appropriate similarity variables can now be determined from the characteristic equations of the group (3.2). These are found by differentiating the relations in (3.2) with respect to a and evaluating the result at the identity element $a = 0$:

$$\frac{dx_i}{x_i} = \frac{dt}{2t} = \frac{du_i}{bu_i} = \frac{dp/\rho}{(b-1)\,p/\rho}. \tag{3.8}$$

Similarity variables found by integrating various combinations of the characteristic equations (3.8) are, in dimensionless form,

$$\left.\begin{aligned} \xi_i = \frac{x_i}{(4\nu t)^{\frac{1}{2}}}; \quad U_i(\xi) = \frac{(n-1)\,u_i}{M(4\nu)^{\frac{1}{2}(1-m)}\, t^{(mk-\frac{1}{2}(m+1))}}, \\ P(\xi) = \frac{(n-1)\,p/\rho}{M(4\nu)^{\frac{1}{2}(2-m)}\, t^{(mk-\frac{1}{2}(m+2))}}. \end{aligned}\right\} \tag{3.9}$$

If we substitute these forms into the full Navier–Stokes equations

$$\left.\begin{aligned} \frac{\partial u_i}{\partial x_i} = 0, \\ \frac{\partial u_i}{\partial t} + \frac{\partial}{\partial x_j}(u_i u_j) + \frac{1}{\rho}\frac{\partial p}{\partial x_i} - \nu \frac{\partial^2 u_i}{\partial x_j \, dx_j} = 0, \end{aligned}\right\} \tag{3.10}$$

the result is $\partial U_i/\partial \xi_i = 0$ and

$$(mk - \tfrac{1}{2}(m+1))\, U_i - \frac{\xi_j}{2}\frac{\partial U_i}{\partial \xi_j} + \frac{\partial P}{\partial \xi_i} - \frac{\partial^2 U_i}{\partial \xi_j \partial \xi_j} = -\left\{\frac{M^{2/m} t^{2k-1}}{(n-1)^{2/m} 4\nu}\right\}^{\frac{1}{2}m} \frac{\partial}{\partial \xi_j}(U_i U_j). \tag{3.11}$$

This exercise has lead to the combination

$$Re = \frac{[I(t)\, t]^{2/m}}{4\nu t} = \frac{M^{2/m} t^{2k-1}}{(n-1)^{2/m} 4\nu} \tag{3.12}$$

as the appropriate Reynolds number for this class of flows. As $Re \to 0$ the Stokes approximation becomes valid. This may correspond to small or large time depending on the value of k.

3.2. *The Euler equations*

It may be mentioned in passing that (3.12) is the appropriate definition of the Reynolds number at all times. To see this we shall digress for a moment and consider the invariance properties of the Euler equations. At high Reynolds number the large-scale structure of turbulent free shear flows is observed to be independent of

ν. In an approximate sense M is the only parameter in the problem and one should expect a similarity solution of the Euler or Reynolds equations

$$\left.\begin{aligned} \frac{\partial u_i}{\partial x_i} &= 0, \\ \frac{\partial u_i}{\partial t} + \frac{\partial}{\partial x_j}(u_i u_j) - \frac{1}{\rho}\frac{\partial p}{\partial x_i} &= 0. \end{aligned}\right\} \tag{3.13}$$

These are invariant under the two-parameter group

$$\left.\begin{aligned} x_i &= \mathrm{e}^{a}\,\hat{x}_i, \\ t &= \mathrm{e}^{a/k}\,\hat{t}, \\ u_i &= \mathrm{e}^{a(k-1)/k}\,\hat{u}_i, \\ \frac{p}{\rho} &= \mathrm{e}^{(2k-2)/k}\,\frac{\hat{p}}{\rho}, \end{aligned}\right\} \tag{3.14}$$

where a and k are arbitrary. Invariance of the impulse integrals (2.29) is assured as long as $k = n/m$ as before. Appropriate similarity variables can now be determined from the characteristic equations of (3.14) for the group parameter a. These are

$$\frac{\mathrm{d}x_i}{x_i} = k\frac{\mathrm{d}t}{t} = \frac{k}{k-1}\frac{\mathrm{d}u_i}{u_i} = \frac{k}{2(k-1)}\frac{\mathrm{d}(p/\rho)}{p/\rho}. \tag{3.15}$$

In dimensionless form the similarity variables, found by integrating various combinations of the equations in (3.15) are

$$\xi_i = \frac{x_i}{M^{1/m}\,t^{k}}; \quad U_i(\xi) = \frac{u_i}{M^{1/m}\,t^{k-1}}; \quad P(\xi) = \frac{p/\rho}{M^{2/m}\,t^{2(k-1)}}. \tag{3.16}$$

Substituting (3.16) into the full Navier–Stokes equations (3.13) gives $\partial U_i/\partial\xi_i = 0$ and

$$(k-1)\,U_i - k\xi_j\frac{\partial U_i}{\partial \xi_j} + \frac{\partial}{\partial \xi_j}(U_i U_j) + \frac{\partial P}{\partial \xi_i} = \left\{\frac{\nu}{M^{2/m}\,t^{2k-1}}\right\}\frac{\partial^2 U_i}{\partial \xi_j\,\partial \xi_j}. \tag{3.17}$$

The expression (3.12) appears again. However in this instance it divides the second derivative term and no regular limit $Re \to \infty$ exists. At this point we should mention the special case $k = \frac{1}{2}$ corresponding to the flow from a round jet with $\boldsymbol{F}(\boldsymbol{x}, t)/\rho = (0, 0, Mu(t))$. In this case the Reynolds number is constant, the stretching groups (3.2) and (3.14) are identical and the reduced equations (3.11) and (3.17) become identical after a rescaling of variables. The ratios of various length and velocity scales are independent of time. This is the one case that admits a similarity solution to the full Navier–Stokes equations at all Reynolds numbers. At high Reynolds number we should expect a solution that is highly complex in space but regular in time. This implies that the chaotic flow observed in real jets is directly associated with instabilities in the neighbourhood of the jet origin.

4. Phase portrait of particle paths

At this point we want to combine the results of the previous sections in a study of the topology of the equations for unsteady particle paths,

$$\frac{\mathrm{d}x_i}{\mathrm{d}t} = u_i(\boldsymbol{x}, t), \tag{4.1}$$

which, when recast in terms of Stokes flow similarity variables (3.9), become

$$\frac{\mathrm{d}\xi_i}{\mathrm{d}\tau} = Re^{\frac{1}{2}m}\, U_i(\xi) - \tfrac{1}{2}\xi_i, \tag{4.2}$$

where $\xi_i = x_i/(4\nu t)^{\frac{1}{2}}$, $\tau = \ln t$ and $m = 4$ for three-dimensional flows and $m = 3$ for two-dimensional flows. The phase portrait of (4.2) corresponds to the vector field defined by the right-hand side of the equations at a fixed value of the Reynolds number. *The topology of this vector field is the primary concern of this paper.* Note that at large radii the equations are dominated by the $-\frac{1}{2}\xi_i$ term and the solution in the far field is a series of rays converging toward the origin. The scaling of coordinates with time brings fluid from infinity into the disturbance region of the jet where it encounters the outwardly diffusing vorticity field. It is often useful to display a flow pattern in this manner and the introduction of a simple descriptor is warranted. In the remaining discussion we shall use the term *entrainment diagram* to refer to the vector field of particle paths in similarity coordinates defined by the phase portrait of (4.2). This term has been used before to denote the use of similarity coordinates to describe mean particle paths of turbulent flows (Cantwell 1981*b*).

4.1. *Invariance with respect to a moving observer*

A useful feature of the entrainment diagram is that it does not depend on the choice of a particular observer. To see this we consider the transformation to moving coordinates

$$\left.\begin{aligned} x_i &= \hat{x}_i - \alpha_i \nu^{\frac{1}{2}} \hat{t}^{\frac{1}{2}}, \\ t &= \hat{t}, \\ u_i &= \hat{u}_i - \tfrac{1}{2}\alpha_i \nu^{\frac{1}{2}} \hat{t}^{-\frac{1}{2}}, \end{aligned}\right\} \tag{4.3}$$

where the α_i are arbitrary dimensionless rates. The similarity velocities (3.9) can be written

$$U_i(\xi) = \frac{u_i}{Re^{\frac{1}{2}m}\, \nu^{\frac{1}{2}}\, t^{-\frac{1}{2}}}. \tag{4.4}$$

In terms of similarity variables, the transformation (4.3) becomes a translation,

$$\left.\begin{aligned} \xi_i &= \hat{\xi}_i - \alpha_i, \\ Re^{\frac{1}{2}m}\, U_i(\xi) &= Re^{\frac{1}{2}m}\, \hat{U}_i(\hat{\xi}) - \tfrac{1}{2}\alpha_i. \end{aligned}\right\} \tag{4.5}$$

When the right-hand side of (4.2) is transformed to new variables using (4.5) the result is

$$Re^{\frac{1}{2}m}\, U_i(\xi) - \tfrac{1}{2}\xi_i = Re^{\frac{1}{2}m}\, \hat{U}_i(\hat{\xi}) - \tfrac{1}{2}\hat{\xi}_i, \tag{4.6}$$

independent of the α_i. The invariance of the vector field of the entrainment diagram under a transformation to an observer moving at a velocity commensurate with the viscous timescale of the flow but with an arbitrary rate is important because it ensures that the phase portrait of (4.2) represents essential structural features of the flow that are not simply a consequence of an arbitrary choice of the frame of reference.

4.2. *Critical points*

The solutions we wish to consider in the next section are most simply posed in spherical polar coordinates (axisymmetric flows) or cylindrical coordinates (planar flows). In both cases the equations for particle paths are

$$\frac{\mathrm{d}r}{\mathrm{d}t} = u(r,\theta,t); \quad \frac{\mathrm{d}\theta}{\mathrm{d}t} = \frac{v(r,\theta,t)}{r}, \tag{4.7}$$

where u and v are the radial and tangential velocities. In terms of similarity variables (3.9)

$$\frac{\mathrm{d}\xi}{\mathrm{d}\tau} = Re^{\frac{1}{2}m}\, U(\xi,\theta) - \tfrac{1}{2}\xi; \quad \frac{\mathrm{d}\theta}{\mathrm{d}\tau} = Re^{\frac{1}{2}m}\frac{V(\xi,\theta)}{\xi}, \tag{4.8}$$

where $\tau = \ln t$ and

$$\left.\begin{aligned} \xi = \frac{r}{(4\nu t)^{\frac{1}{2}}}; \quad U(\xi,\theta) &= \frac{(n-1)\,u(r,\theta,t)}{M(4\nu)^{\frac{1}{2}(1-m)}\, t^{mk-\frac{1}{2}(m+1)}}, \\ V(\xi,\theta) &= \frac{(n-1)\,v(r,\theta,t)}{M(4\nu)^{\frac{1}{2}(1-m)}\, t^{mk-\frac{1}{2}(m+1)}}, \end{aligned}\right\} \tag{4.9}$$

and

$$Re = \frac{M^{2/m}\, t^{2k-1}}{(n-1)^{2/m}\, 4\nu}. \tag{4.10}$$

The equations (4.8) are strictly autonomous only for $k = \frac{1}{2}$. Critical points (ξ_c, θ_c) of (4.8) occur where

$$Re^{\frac{1}{2}m} = \frac{\xi_c}{2U(\xi_c,\theta_c)}; \quad V(\xi_c,\theta_c) = 0. \tag{4.11}$$

Near a critical point (4.8) may be expanded as

$$\begin{bmatrix} \dfrac{\mathrm{d}\xi}{\mathrm{d}\tau} \\ \dfrac{\mathrm{d}\theta}{\mathrm{d}\tau} \end{bmatrix} = \begin{bmatrix} a & b \\ c & d \end{bmatrix} \begin{bmatrix} \xi-\xi_c \\ \theta-\theta_c \end{bmatrix} = \boldsymbol{B} \begin{bmatrix} \xi-\xi_c \\ \theta-\theta_c \end{bmatrix} \tag{4.12}$$

as long as the flow is regular in the neighbourhood of (ξ_c, θ_c). The coefficients of the matrix $\boldsymbol{B}$ are related to the first partial derivatives of (4.8) evaluated at the critical point.

$$\left.\begin{aligned} a &= Re^{\frac{1}{2}m}\frac{\partial U}{\partial \xi}\bigg|_{(\xi_c,\,\theta_c)} - \tfrac{1}{2}, \\ b &= Re^{\frac{1}{2}m}\frac{\partial U}{\partial \theta}\bigg|_{(\xi_c,\,\theta_c)}, \\ c &= Re^{\frac{1}{2}m}\frac{\partial}{\partial \xi}\left(\frac{V}{\xi}\right)\bigg|_{(\xi_c,\,\theta_c)}, \\ d &= Re^{\frac{1}{2}m}\frac{\partial U}{\partial \theta}\left(\frac{V}{\xi}\right)\bigg|_{(\xi_c,\,\theta_c)}. \end{aligned}\right\} \tag{4.13}$$

The topology of the flow in the neighbourhood of the critical point is determined by the two invariants p and q where

$$p = -(a+d), \quad q = ad - bc. \tag{4.14}$$

The eigenvalues of the matrix $\boldsymbol{B}$ satisfy the characteristic equation $\lambda^2 + p\lambda + q = 0$ with roots $\lambda = -\frac{1}{2}p \pm \frac{1}{2}[(p^2+q)^{\frac{1}{2}}]$. If (p,q) lies above the parabola $q = \frac{1}{4}p^2$ the eigenvalues are complex-conjugates and the local trajectories form a stable focus. If (p,q) lies below $q = \frac{1}{4}p^2$ but above $q = 0$ the critical point is a node and if $q < 0$ the critical point is a saddle.

4.3. *Continuity*

In general p, q, ξ_c and θ_c depend on Re and the possibility of a bifurcation in the entrainment diagram follows. When continuity is applied to the flow near the critical point a certain relationship is imposed between p and q. The axisymmetric case will be treated first. In spherical polar coordinates the continuity equation is

$$2U+\xi\frac{\partial U}{\partial \xi}+\frac{\cos\theta}{\sin\theta}V+\frac{\partial V}{\partial\theta}=0. \tag{4.15}$$

Near a critical point (ξ_c,θ_c),

$$\left.\begin{aligned} Re^2\,U &= \tfrac{1}{2}\xi+a(\xi-\xi_c)+b(\theta-\theta_c),\\ Re^2\,V &= c\xi(\xi-\xi_c)+d\xi(\theta-\theta_c). \end{aligned}\right\} \tag{4.16}$$

Substituting (4.16) into (4.15) and taking the limit $\xi\to\xi_c$, $\theta\to\theta_c$ we see that there are two possible cases:

case 1. $\theta_c\neq 0$

$$p=\tfrac{3}{2}\quad\text{(three-dimensional flows)}; \tag{4.17}$$

case 2. $\theta_c=0$, $c=0$. Substituting $p=\frac{3}{2}+d$ along with $a=-\frac{3}{2}-2d$ into $q=ad$ gives

$$q=(p-\tfrac{3}{2})(\tfrac{3}{2}-2p)\quad\text{(three dimensional flows)}. \tag{4.18}$$

Any on-axis critical point must lie on the parabola in (p,q)-coordinates given by (4.18). Any off-axis critical point will follow the line $p=\frac{3}{2}$.

For the case of planar flows, the continuity equation in cylindrical coordinates is

$$U+\xi\frac{\partial U}{\partial\xi}+\frac{\partial V}{\partial\theta}=0. \tag{4.19}$$

Near a critical point (ξ_c,θ_c)

$$\left.\begin{aligned} Re^{\frac{3}{2}}\,U &= \tfrac{1}{2}\xi+a(\xi-\xi_c)+b(\theta-\theta_c),\\ Re^{\frac{3}{2}}\,V &= c\xi(\xi-\xi_c)+d\xi(\theta-\theta_c). \end{aligned}\right\} \tag{4.20}$$

Substituting (4.20) into (4.19) and taking the limit $\xi\to\xi_c$, $\theta\to\theta_c$ gives

$$p=1\quad\text{(two-dimensional flows)}. \tag{4.21}$$

Any critical point must lie on the line $p=1$. Thus the value of p is fixed by continuity and the dimensionality of the space in which the flow is imbedded. These results follow only from considerations of continuity and the form of the particle-path equations (4.8).

The quantity q involves products of derivatives of the velocity field and can be related to the vorticity and strain at the critical point. For axisymmetric flows

$$q=\tfrac{1}{4}Re^4\{[W_\phi(\xi_c,\theta_c)]^2-\Phi(\xi_c,\theta_c)\}+(p-\tfrac{3}{2})\,p+\tfrac{3}{4}, \tag{4.22}$$

and for planar flows

$$q=\tfrac{1}{4}Re^4\{[W_z(\xi_c,\theta_c)]^2-\Phi(\xi_c,\theta_c)\}+\tfrac{1}{4}, \tag{4.23}$$

where the definitions of vorticity and strain in cylindrical and spherical polar coordinates have been used. The dissipation of kinetic energy is $\epsilon=\nu\phi$ where $\phi=S_{ij}S_{ij}$ and S_{ij} is the rate-of-strain tensor. The quantity ϕ is related to Φ by $\phi=M^2(4\nu)^{-m}\,t^{2mk-m-2}\,\Phi$. Equations (4.22) and (4.23) show that the topology of the flow near a critical point is determined by a balance between rotation and strain. If

$\Phi > W^2$ strain dominates rotation and the solution trajectories of (4.8) near (ξ_c, θ_c) will be nodal-like or saddle-like. If $W^2 > \Phi$ the trajectories near the point will form a stable focus. The focus does not have to involve a local maximum in W. All that is required is that rotation dominate strain.

5. Limiting behaviour at large and small radius

At this point we have determined the shape of the (p, q)-trajectory for the class of flows under study. There are certain important cases where ξ_c and θ_c depend on Re but p and q do not. These usually represent limiting cases of an overall solution and they can be used to assign endpoints to the trajectory of the overall solution on the (p, q)-plane, thus completing the specification of the topology of the flow.

5.1. *The limit* $\xi \to \infty$

All of the flows studied in this paper behave like a dipole in the far field with vector potentials given by

$$\left.\begin{aligned} A_\phi &= \frac{I(t)}{4\pi}\frac{\sin\theta}{r^2} \quad \text{(axisymmetric)},\\ A_z &= \frac{I(t)}{4\pi}\frac{\sin\theta}{r} \quad \text{(planar)}. \end{aligned}\right\} \tag{5.1}$$

The impulse integrals (2.29) are substituted into (5.1) and the result is differentiated to obtain velocities. The resulting particle-path equations for the far-field flow are

$$\left.\begin{aligned} \frac{d\xi}{d\tau} &= Re^2\left\{\frac{1}{2\pi}\frac{\cos\theta}{\xi^3}\right\} - \tfrac{1}{2}\xi\\ \frac{d\theta}{d\tau} &= Re^2\left\{\frac{1}{4\pi}\frac{\sin\theta}{\xi^4}\right\} \end{aligned}\right\} \quad \text{(axisymmetric)}, \tag{5.2}$$

and

$$\left.\begin{aligned} \frac{d\xi}{d\tau} &= Re^{\frac{3}{2}}\left\{\frac{1}{2\pi}\frac{\cos\theta}{\xi^2}\right\} - \tfrac{1}{2}\xi\\ \frac{d\theta}{d\tau} &= Re^{\frac{3}{2}}\left\{\frac{1}{4\pi}\frac{\sin\theta}{\xi^3}\right\} \end{aligned}\right\} \quad \text{(planar)}. \tag{5.3}$$

The system (5.2) has a critical point on the jet axis at $(\xi_c, \theta_c) = (Re^{\frac{1}{2}}/(\pi)^{\frac{1}{4}}, 0)$ and in the neighbourhood of this point

$$\begin{bmatrix} \frac{d\xi}{d\tau} \\ \frac{d\theta}{d\tau} \end{bmatrix} = \begin{bmatrix} -2 & 0 \\ 0 & \frac{1}{4} \end{bmatrix}\begin{bmatrix} \xi-\xi_c \\ \theta-\theta_c \end{bmatrix}. \tag{5.4}$$

The critical point is a saddle at $p = \frac{7}{4}$, $q = -\frac{1}{2}$ and lies on the parabola (4.18); see figure 2(*a*). The system (5.3) has a critical point at $(\xi_c, \theta_c) = (Re^{\frac{1}{2}}/(2\pi)^{\frac{1}{3}}, 0)$ and in the neighbourhood of this point

$$\begin{bmatrix} \frac{d\xi}{d\tau} \\ \frac{d\theta}{d\tau} \end{bmatrix} = \begin{bmatrix} -\frac{3}{2} & 0 \\ 0 & \frac{1}{2} \end{bmatrix}\begin{bmatrix} \xi-\xi_c \\ \theta-\theta_c \end{bmatrix}. \tag{5.5}$$

In this case the critical point is also a saddle but with $p = 1$, as expected from our considerations of two-dimensional continuity, and $q = -\frac{3}{4}$; see figure 2(*b*). In §6 solutions for the six cases ($k = \frac{1}{4}, \frac{1}{2}, \frac{3}{4}$; axisymmetric and $k = \frac{1}{3}, \frac{2}{3}, 1$; planar) are summarized. To the extent that these overall solutions approach the dipole behaviour (5.1) when ξ is large, one may expect that the on-axis critical points of these solutions will approach the dipole behaviour of the critical points of (5.4) and (5.5) when the Reynolds number is large. In general one can associate large values of ξ_c with large values of Re and in some circumstances it is convenient to replace one limiting process by the other. This is just a consequence of the fact that the radius, ξ_c, at which the outwardly directed velocity term and inwardly directed coordinate term in (4.2) are in balance must increase as Re is increased.

5.2. *The limit* $\xi \to 0$

(i) *Axisymmetric cases* ($k = \frac{1}{4}, \frac{1}{2}, \frac{3}{4}$)

The solutions we wish to study are obtained by solving the diffusion equation for the vorticity in spherical polar coordinates

$$\frac{\partial \omega_\phi}{\partial t} = \nu \left\{ \frac{1}{r^2} \frac{\partial}{\partial \theta} \left(\frac{1}{\sin\theta} \frac{\partial}{\partial \theta} (\omega_\phi \sin\theta) \right) + \frac{1}{r} \frac{\partial^2}{\partial r^2} (r\omega_\phi) \right\}. \tag{5.6}$$

Similarity forms for the vorticity and stream function are

$$\Psi_\phi(\xi, \theta) = \frac{(n-1)\,\psi_\phi(r, \theta, t)}{M(4\nu)^{-\frac{1}{2}} t^{4k-\frac{3}{2}}}, \quad W_\phi(\xi, \theta) = \frac{(n-1)\,\omega_\phi(r, \theta, t)}{M(4\nu)^{-2} t^{4k-3}}. \tag{5.7}$$

In the limit $Re \to 0$ the stream function and vorticity are symmetric about the equatorial plane $z = 0$. Let

$$W_\phi = \sin\theta\, f_1(\xi); \quad \Psi_\phi = \sin^2\theta\, g_1(\xi). \tag{5.8}$$

The velocity is related to the stream function by

$$U(\xi, \theta) = \frac{1}{\xi^2 \sin\theta} \frac{\partial \Psi_\phi}{\partial \theta}; \quad V(\xi, \theta) = -\frac{1}{\xi \sin\theta} \frac{\partial \Psi_\phi}{\partial \xi} \tag{5.9}$$

and the radial functions f_1 and g_1 are related through (5.9) and the continuity equation (4.15):

$$\frac{\mathrm{d}}{\mathrm{d}\xi} \left[\frac{1}{\xi^2} \frac{\mathrm{d}}{\mathrm{d}\xi} (\xi g_1) \right] = -f_1. \tag{5.10}$$

Substituting the expression for vorticity from (5.9) into (5.6) leads to the governing ordinary differential equation for the axisymmetric cases:

$$\xi^2 \frac{\mathrm{d}^2 f_1}{\mathrm{d}\xi^2} + 2\xi(\xi^2+1) \frac{\mathrm{d}f_1}{\mathrm{d}\xi} - [4(4k-3)\,\xi^2 + 2] f_1 = 0. \tag{5.11}$$

Solutions of (5.11) are given in the next section but for the present we want to focus on the limit $\xi \to 0$. In this limit

$$\xi^2 \frac{\mathrm{d}^2 f_1}{\mathrm{d}\xi^2} + 2\xi \frac{\mathrm{d}f_1}{\mathrm{d}\xi} - 2f_1 = 0, \tag{5.12}$$

independent of k. Equation (5.12) has two solutions:

$$f_1 = \xi; \quad g_1 = c_1 \xi^2 + c_2 \xi^4, \tag{5.13}$$

and

$$f_1 = \xi^{-2}; \quad g_1 = c_1 \xi + c_2 \xi^2, \tag{5.14}$$

where (5.10) has been used to solve for g_1. The constants of integration c_1 and c_2 are undetermined at this point. The non-singular solution (5.13) applies to cases for which the applied force is zero for $t > 0$, for example the vortex ring ($k = \frac{1}{4}$). The particle-path equations (4.8) for this case are

$$\left.\begin{aligned} \frac{d\xi}{d\tau} &= Re^2[2c_1\cos\theta] - \tfrac{1}{2}\xi \\ \frac{d\theta}{d\tau} &= Re^2\left[-2c_1\frac{\sin\theta}{\xi}\right] \end{aligned}\right\} \quad (k = \tfrac{1}{4}). \tag{5.15}$$

This system has a critical point on the jet axis at $(\xi_c, \theta_c) = (4c_1 Re^2, 0)$, and in the neighbourhood of this point

$$\begin{bmatrix} \frac{d\xi}{d\tau} \\ \frac{d\theta}{d\tau} \end{bmatrix} = \begin{bmatrix} -\frac{1}{2} & 0 \\ 0 & \frac{1}{2} \end{bmatrix} \begin{bmatrix} \xi - \xi_c \\ \theta - \theta_c \end{bmatrix}. \tag{5.16}$$

The critical point of the system (5.16) is a star node at $(p, q) = (1, \frac{1}{4})$ and lies at the point of osculation of the parabola (4.18) and the parabola $q = \frac{1}{4}p^2$; see figure 2(*a*). This result is typical in that the system (5.16) is independent of the constant of integration c_1. The singular solution (5.14) applies to cases for which the applied force remains on for $t > 0$; the round jet ($k = \frac{1}{2}$) and ramp jet ($k = \frac{3}{4}$). The limiting particle-path equations for these cases are

$$\left.\begin{aligned} \frac{d\xi}{d\tau} &= Re^2\left[2c_1\frac{\cos\theta}{\xi}\right] - \tfrac{1}{2}\xi \\ \frac{d\theta}{d\tau} &= Re^2\left[-c_1\frac{\sin\theta}{\xi^2}\right] \end{aligned}\right\} \quad (k = \tfrac{1}{2}, \tfrac{3}{4}). \tag{5.17}$$

The system (5.17) has a critical point on the jet axis at $(\xi_c, \theta_c) = 2(c_1)^{\frac{1}{2}} Re$ and in the neighbourhood of this point

$$\begin{bmatrix} \frac{d\xi}{d\tau} \\ \frac{d\theta}{d\tau} \end{bmatrix} = \begin{bmatrix} -1 & 0 \\ 0 & -\frac{1}{4} \end{bmatrix} \begin{bmatrix} \xi - \xi_c \\ \theta - \theta_c \end{bmatrix}. \tag{5.18}$$

The critical point is a node at $(p, q) = (\frac{5}{4}, \frac{1}{4})$ and lies on the parabola (4.18).

(ii) *Planar cases* ($k = \frac{1}{3}, \frac{2}{3}, 1$)

We need to solve the vorticity diffusion equation in cylindrical polar coordinates:

$$\frac{\partial\omega_z}{\partial t} = \nu\left\{\frac{1}{r}\frac{\partial}{\partial r}\left(r\frac{\partial\omega_z}{\partial r}\right) + \frac{1}{r^2}\frac{\partial^2\omega_z}{\partial\theta^2}\right\}. \tag{5.19}$$

Similarity forms for the vorticity and stream function are

$$\Psi_z(\xi, \theta) = \frac{(n-1)\,\psi_z(r, \theta, t)}{M(4\nu)^{-\frac{1}{2}} t^{3k-\frac{3}{2}}}, \quad W_z(\xi, \theta) = \frac{(n-1)\,\omega_z(r, \theta, t)}{M(4\nu)^{-\frac{3}{2}} t^{3k-\frac{5}{2}}}. \tag{5.20}$$

As before the stream function and vorticity are symmetric about the vertical plane $x = 0$ in the Stokes limit and we search for solutions of the form

$$W_z = \sin\theta\, f_2(\xi); \quad \Psi_z = \sin\theta\, g_2(\xi). \tag{5.21}$$

The velocity is related to the stream function by

$$U(\xi,\theta)=\frac{1}{\xi}\frac{\partial \Psi_z}{\partial\theta};\quad V(\xi,\theta)=-\frac{\partial \Psi_z}{\partial\xi}, \tag{5.22}$$

and the radial functions f_2 and g_2 are related through (5.22) and the continuity equation (4.19):

$$\frac{\mathrm{d}}{\mathrm{d}\xi}\left(\frac{1}{\xi}\frac{\mathrm{d}}{\mathrm{d}\xi}(\xi g_2)\right)=-f_2. \tag{5.23}$$

The expression for vorticity (5.21) is substituted into (5.19) to obtain the governing ordinary differential equation for the planar cases:

$$\xi^2\frac{\mathrm{d}^2 f_2}{\mathrm{d}\xi^2}+\xi(2\xi^2+1)\frac{\mathrm{d}f_2}{\mathrm{d}\xi}-[4(3k-\tfrac{5}{2})\xi^2+1]f_2=0. \tag{5.24}$$

Solutions of (5.24) will be given shortly but, as before, we first want to look at the limit $\xi\to 0$. In this limit (5.24) becomes

$$\xi^2\frac{\mathrm{d}^2 f_2}{\mathrm{d}\xi^2}+\xi\frac{\mathrm{d}f_2}{\mathrm{d}\xi}-f_2=0, \tag{5.25}$$

again independent of k. The two solutions of (5.24) are

$$f_2=\xi;\quad g_2=c_1\xi+c_2\xi^3, \tag{5.26}$$

and

$$f_2=\xi^{-1};\quad g_2=c_1\xi\ln\xi+c_2\xi, \tag{5.27}$$

where c_1 and c_2 are unknown constants. The non-singular solution (5.26) applies to the vortex pair ($k=\frac{1}{3}$). For this case the particle path equations (4.8) are

$$\left.\begin{aligned}\frac{\mathrm{d}\xi}{\mathrm{d}\tau}&=Re^{\frac{3}{2}}\{c_1\cos\theta\}-\tfrac{1}{2}\xi\\ \frac{\mathrm{d}\theta}{\mathrm{d}\tau}&=Re^{\frac{3}{2}}\left\{-c_1\frac{\sin\theta}{\xi}\right\}\end{aligned}\right\}\quad(k=\tfrac{1}{3}). \tag{5.28}$$

This system has a critical point on the jet axis at $(\xi_c,\theta_c)=(2c_1 Re^{\frac{3}{2}},0)$ and in the neighbourhood of this point

$$\begin{bmatrix}\frac{\mathrm{d}\xi}{\mathrm{d}\tau}\\ \frac{\mathrm{d}\theta}{\mathrm{d}\tau}\end{bmatrix}=\begin{bmatrix}-\frac{1}{2} & 0\\ 0 & -\frac{1}{2}\end{bmatrix}\begin{bmatrix}\xi-\xi_c\\ \theta-\theta_c\end{bmatrix}. \tag{5.29}$$

As in the case of the $\xi\to 0$ limit of the vortex ring ($k=\frac{1}{4}$) the limiting critical point of the vortex pair is a star node at $(p,q)=(1,\frac{1}{4})$ and lies on the parabola $q=\frac{1}{4}p^2$; see figure 2(*b*). The singular solution (5.27) applies to the plane jet and plane ramp jet and for these cases

$$\left.\begin{aligned}\frac{\mathrm{d}\xi}{\mathrm{d}\tau}&=Re^{\frac{3}{2}}\{c_1\cos\theta\ln\xi\}-\tfrac{1}{2}\xi\\ \frac{\mathrm{d}\theta}{\mathrm{d}\tau}&=Re^{\frac{3}{2}}\left\{-c_1\sin\theta\frac{\ln\xi}{\xi}\right\}\end{aligned}\right\}\quad(k=\tfrac{2}{3},1). \tag{5.30}$$

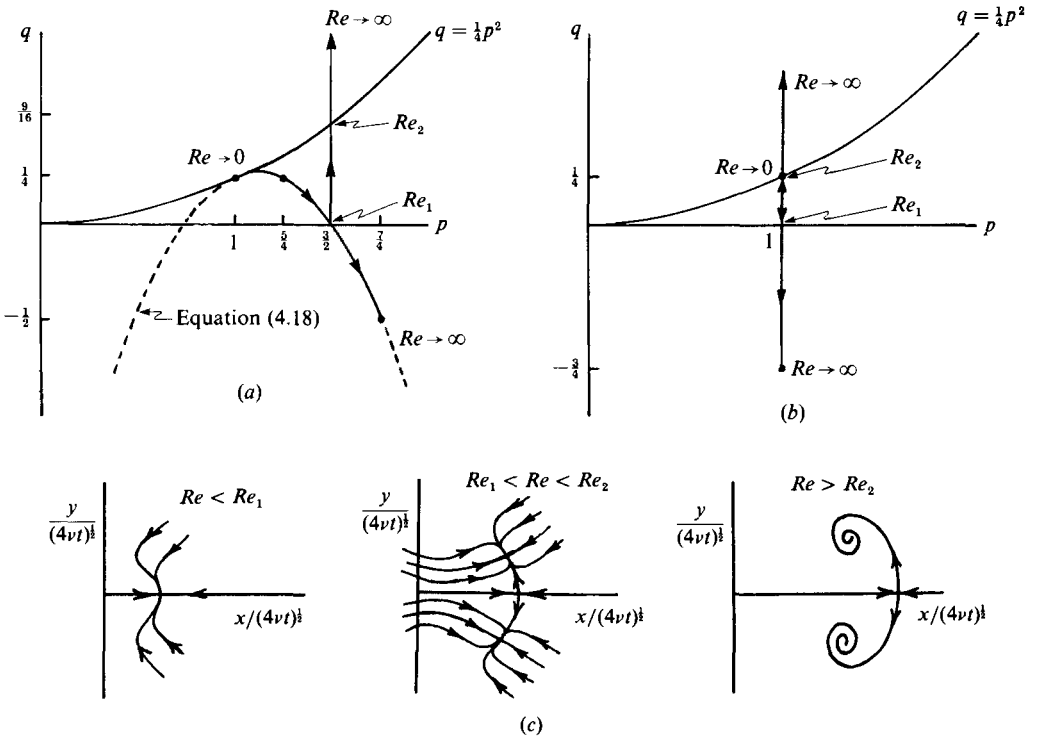

FIGURE 2. Critical-point trajectories in the (p, q)-plane. (a) Axisymmetric jets; $Re \to 0$ limit is $(p, q) = (1, \frac{1}{4})$ for $k = \frac{1}{4}$ and $(p,q) = (\frac{5}{4}, \frac{1}{4})$ for $k = \frac{1}{2}, \frac{3}{4}$. ($b$) Planar jets; $Re \to 0$ limit is $(p, q) = (1, \frac{1}{4})$ for $k = \frac{1}{3}, \frac{2}{3}, 1$. ($c$) Schematic entrainment diagrams depicting three states of motion. See table 1 for values of Re_1 and Re_2.

The system (5.30) has a critical point on the jet axis at $(\xi_c, \theta_c) = (2c_1 Re^{\frac{3}{2}}, 0)$ and in the neighbourhood of this point

$$\begin{bmatrix} \frac{d\xi}{d\tau} \\ \frac{d\theta}{d\tau} \end{bmatrix} = \begin{bmatrix} \frac{1}{2\ln\xi_c} - \frac{1}{2} & 0 \\ 0 & -\frac{1}{2\ln\xi_c} - \frac{1}{2} \end{bmatrix} \begin{bmatrix} \xi - \xi_c \\ \theta - \theta_c \end{bmatrix}. \tag{5.31}$$

In this case $p = 1$ but q depends on the Reynolds number and c_1 through the logarithm which appears in (5.31). As $Re \to 0$, $\xi_c \to 0$ and the point approaches a star node at $(p, q) = (1, \frac{1}{4})$; however in this limit a regular expansion about the critical point does not exist owing to the essential singularity.

5.5. *The (p, q)-trajectory*

Figure 2(a, b) depicts the (p, q)-trajectories for the six jet flows studied. The arrows on the trajectories represent the direction of increasing Reynolds number. All six cases involve two critical Reynolds numbers and three distinct states of motion illustrated by the entrainment diagrams shown schematically in figure 2(c). Below the first critical Reynolds number Re_1, the entrainment diagram consists of a single stable node on the flow axis as deduced from the $\xi \to 0$ limit. As the Reynolds number

is increased above Re_1 the stable node splits to form an off-axis node and on-axis saddle. The condition for the first bifurcation is

$$q(Re_1) = 0, \quad \theta_c = 0. \tag{5.32}$$

As the Reynolds number is further increased above the second critical value Re_2 the off-axis node becomes a stable focus. The condition for the second bifurcation is:

$$\left.\begin{aligned} q(Re_2) &= \tfrac{9}{16}, \quad \theta_c \neq 0 \quad \text{(axisymmetric)} \\ q(Re_2) &= \tfrac{1}{4}, \quad \theta_c \neq 0 \quad \text{(planar)} \end{aligned}\right\}. \tag{5.33}$$

At this point, considerations of continuity and the limiting behaviour of the solutions have generated a fairly complete topological picture of the starting process for two- and three-dimensional jets and this is about as far as we can go without considering complete solutions. The missing elements are the actual values of Re_1 and Re_2. In general this requires a solution of the complete equations of motion. However the analysis of (4.15)–(4.21) does not depend on the particular time dependence of the velocity field implied by the similarity form of the heat equation given by (4.4). The time dependence could be much more complicated. The implication of this is that the critical points in the entrainment diagram of the axisymmetric or planar nonlinear solution must also follow the same (p, q)-trajectory as the Stokes solution and one may expect a series of flow states topologically similar to those in figure 2(*c*). In this respect we may use overall solutions of the Stokes equations to give us a first cut at the values of Re_1 and Re_2.

6. Stokes solutions

Complete solutions of the ordinary differential equations (5.11) and (5.24) governing the radial vorticity are determined using the Frobenius method. Equations (5.10) and (5.23) are then integrated twice to obtain the radial stream function. The axisymmetric solutions are

(i) *The vortex ring*: $F(t)/\rho = M\delta(t)$, $k = \frac{1}{4}$

$$f_1(\xi) = \frac{2}{\pi^{\frac{3}{2}}}(\xi)\,e^{-\xi^2}, \tag{6.1}$$

$$g_1(\xi) = \frac{1}{4\pi}\left(\frac{1}{\xi}\right)\left\{\operatorname{erf}(\xi) - \frac{2\xi}{\pi^{\frac{1}{2}}}e^{-\xi^2}\right\}. \tag{6.2}$$

(ii) *The round jet*: $F(t)/\rho = Mh(t)$, $k = \frac{1}{2}$

$$f_1(\xi) = \frac{1}{\pi}\left(\frac{1}{\xi^2}\right)\left\{\frac{2\xi}{\pi^{\frac{1}{2}}}e^{-\xi^2} + 1 - \operatorname{erf}(\xi)\right\}, \tag{6.3}$$

$$g_1(\xi) = \frac{1}{4\pi}\left(\frac{1}{\xi}\right)\left\{2\xi^2 - \frac{2\xi}{\pi^{\frac{1}{2}}}e^{-\xi^2} - (2\xi^2 - 1)\operatorname{erf}(\xi)\right\}. \tag{6.4}$$

(iii) *The ramp jet*: $F(t)/\rho = Mth(t)$, $k = \frac{3}{4}$

$$f_1(\xi) = \frac{1}{\pi}\left(\frac{2}{\xi^2}\right)\left\{(1 - 2\xi^2)(1 - \operatorname{erf}(\xi)) + \frac{2\xi}{\pi^{\frac{1}{2}}}e^{-\xi^2}\right\}, \tag{6.5}$$

$$g_1(\xi) = \frac{1}{4\pi}\left(\frac{4}{\xi}\right)\left\{\xi^2(\xi^2 + 1)(1 - \operatorname{erf}(\xi)) + \tfrac{1}{4}\operatorname{erf}(\xi) - \frac{2\xi}{\pi^{\frac{1}{2}}}(\xi^2 + \tfrac{1}{2})e^{-\xi^2}\right\}. \tag{6.6}$$

These solutions involve the error function

$$\operatorname{erf}(\xi) = \frac{2}{\pi^{\frac{1}{2}}} \int_0^{\xi} \mathrm{e}^{-x^2}\, \mathrm{d}x, \tag{6.7}$$

with limiting behaviour

$$\left.\begin{aligned} \lim_{\xi \to 0} \operatorname{erf}(\xi) &= \frac{2}{\pi^{\frac{1}{2}}} \left\{ \xi - \frac{\xi^3}{3} + \frac{\xi^5}{10} - \frac{\xi^7}{42} \cdots \right\}, \\ \lim_{\xi \to \infty} \operatorname{erf}(\xi) &= 1 - \frac{1}{\pi^{\frac{1}{2}}} \frac{\mathrm{e}^{-\xi^2}}{\xi} + \frac{1}{2\pi^{\frac{1}{2}}} \frac{\mathrm{e}^{-\xi^2}}{\xi^3} - \cdots . \end{aligned}\right\} \tag{6.8}$$

The solution for the vortex ring (6.1) is the simple dipole solution of the heat equation. The solution for the round jet (6.4) may be found in the paper by Sozou (1979) and the ramp jet (6.6) was worked out by Allen (1984) as one of a large class of forced axisymmetric Stokes flow solutions. Solutions of (5.24) are complicated somewhat by the logarithmic singularity which appears when $k \geqslant \frac{2}{3}$. The Frobenius method can still be carried through and the results for the planar cases are

(iv) *The vortex pair*: $F(t)/\rho = M\delta(t)$, $k = \frac{1}{3}$

$$f_2(\xi) = \frac{1}{\pi}(\xi)\, \mathrm{e}^{-\xi^2}, \tag{6.9}$$

$$g_2(\xi) = \frac{1}{4\pi}\left(\frac{1}{\xi}\right)(1 - \mathrm{e}^{-\xi^2}). \tag{6.10}$$

(v) *The plane jet*: $F(t)/\rho = Mh(t)$, $k = \frac{2}{3}$

$$f_2(\xi) = \frac{1}{\pi}\left(\frac{1}{\xi}\right) \mathrm{e}^{-\xi^2}, \tag{6.11}$$

$$g_2(\xi) = \frac{1}{4\pi}\left(\frac{1}{\xi}\right)\{1 - \mathrm{e}^{-\xi^2} + \xi^2 E_1(\xi^2)\}. \tag{6.12}$$

(vi) *The plane ramp jet*: $F(t)/\rho = Mth(t)$, $k = 1$

$$f_2(\xi) = \frac{1}{\pi}\left(\frac{2}{\xi}\right)\{\mathrm{e}^{-\xi^2} - \xi^2 E_1(\xi^2)\}, \tag{6.13}$$

$$g_2(\xi) = \frac{1}{4\pi}\left(\frac{2}{\xi}\right)\{\tfrac{1}{2} - \tfrac{1}{2}(1 + \xi^2)\, \mathrm{e}^{-\xi^2} + (1 + \tfrac{1}{2}\xi^2)\, \xi^2 E_1(\xi^2)\}. \tag{6.14}$$

The solution for the vortex pair is again the simple dipole solution of the heat equation. The plane-jet and plane-ramp-jet cases involve the exponential integral

$$E_1(\xi^2) = \int_{\xi^2}^{\infty} \frac{\mathrm{e}^{-x}}{x}\, \mathrm{d}x \tag{6.15}$$

with limiting behaviour

$$\left.\begin{aligned} \lim_{\xi \to 0} E_1(\xi^2) &= -\gamma - \ln(\xi^2) + \xi^2 - \tfrac{1}{4}\xi^4 + \tfrac{1}{18}\xi^6 - \tfrac{1}{48}\xi^8 + \cdots, \\ \lim_{\xi \to \infty} E_1(\xi^2) &= \frac{1}{\xi^2}\, \mathrm{e}^{-\xi^2}, \end{aligned}\right\} \tag{6.16}$$

where γ is Euler's constant, $\gamma = 0.5772156649$.

Figure 3 depicts contour plots of the self-similar stream function for the various cases. The pronounced convergence of streamlines in the neighbourhood of the origin

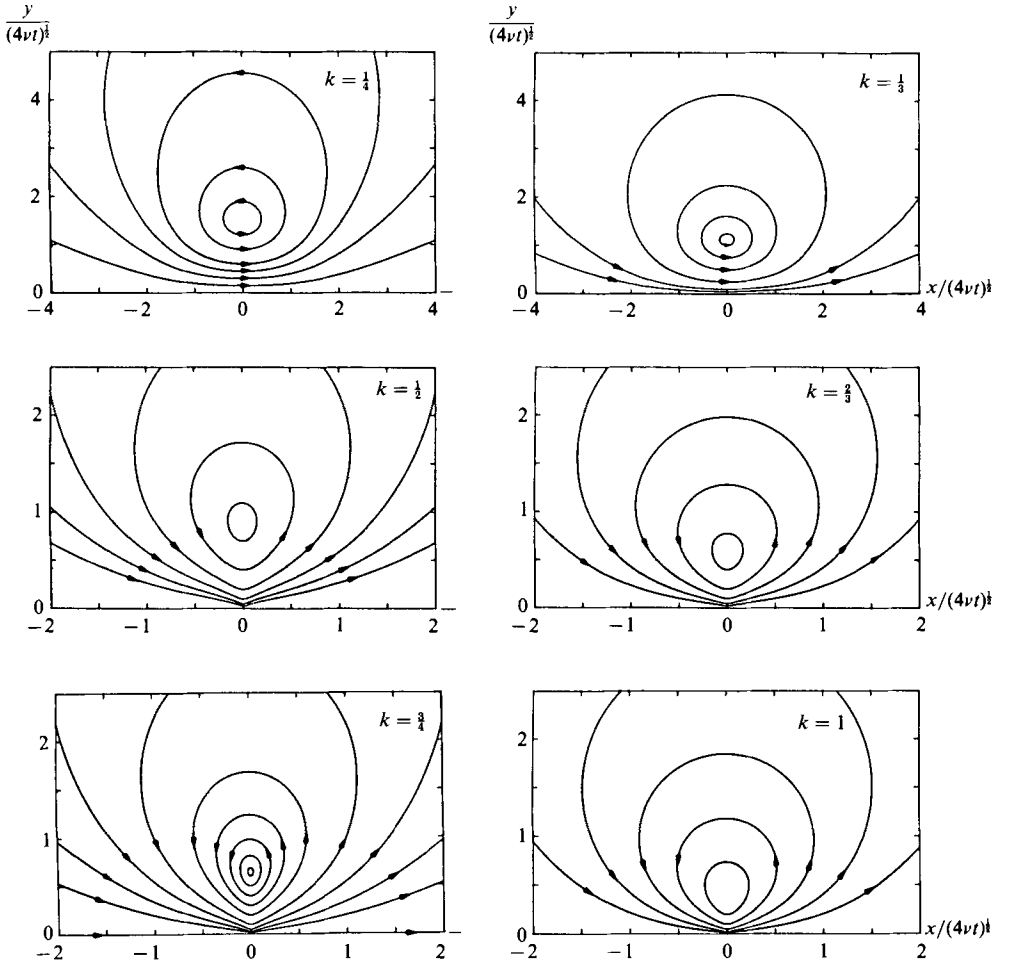

FIGURE 3. Contour lines of the self-similar stream function, Ψ.

Flow	k	ξ_0	Re_1	Re_2
Vortex ring	$\frac{1}{4}$	1.47172	4.5437	5.8526
Round jet	$\frac{1}{2}$	0.88165	1.6951	2.5227
Ramp jet	$\frac{3}{4}$	0.64153	0.9347	1.4472
Vortex pair	$\frac{1}{3}$	1.12091	3.3695	3.8818
Plane jet	$\frac{2}{3}$	0.56689	1.6307	2.1945
Plane ramp jet	1	0.40300	0.8751	1.2086

TABLE 1

for the cases with $k \geqslant \frac{1}{2}$ is evidence of the singularity in the velocity at that point. In all cases the tangential velocity has a root ξ_0 at which $V(\xi_0, \theta) = 0$ for all θ. This root, combined with the antisymmetry of the radial velocity about the vertical axis, leads to the closed-centre characteristic of a dipole-like flow, The variation of the radius of the point of maximum stream function from case to case reflects the dependence of ξ_0 on k shown in table 1. In general ξ_0 decreases as k increases for a given

geometry of forcing (given m). For a given type of forcing (given n) the root is smaller for line forcing ($m = 3$) than for point forcing ($m = 4$). In physical coordinates the closed centre moves vertically upward at a rate proportional to $1/t^{\frac{1}{2}}$ and independent of the Reynolds number. As time progresses a given streamline will grow and move outward as the vorticity field diffuses away from the origin. Except for the scaling in time the *pattern* of streamlines is independent of the Reynolds number.

Radial distributions of vorticity are shown in figure 4. The non-singular cases of the vortex ring and vortex pair have a maximum at a radius that lies well inside the maximum in the stream function. In the singular cases the vorticity is proportional to $1/\xi^2$ near the origin then dies off exponentially and is essentially negligible beyond $\xi = 2$ in all six cases.

6.1. *Regions of validity*

Before the specification of these solutions can be considered complete we need to check the validity of the Stokes approximation over the range of the radial coordinate. This involves using the Stokes solutions to estimate the order of magnitude of the acceleration, pressure, nonlinear-convective and viscous terms in the Navier–Stokes equations (3.10) or their reduced form (3.11). Note that in the Stokes approximation, the expression for the far-field pressure given by (2.20) is valid over $0 \leqslant \xi < \infty$ since in this limit the pressure satisfies the Laplace equation. At large ξ

$$U_i \sim \frac{1}{\xi^3}; \quad \frac{\partial P}{\partial \xi} \sim \frac{1}{\xi^3}; \quad \frac{\partial}{\partial \xi_j}(U_i U_j) \sim \frac{Re^2}{\xi^7}; \quad \frac{\partial^2 U_i}{\partial \xi_j \partial \xi_j} \sim \frac{1}{\xi^5} \quad \text{(axisymmetric)}, \tag{6.17}$$

$$U_i \sim \frac{1}{\xi^2}; \quad \frac{\partial P}{\partial \xi_i} \sim \frac{1}{\xi^2}; \quad \frac{\partial}{\partial \xi_j}(U_i U_j) \sim \frac{Re^{\frac{3}{2}}}{\xi^5}; \quad \frac{\partial^2 U_i}{\partial \xi_j \partial \xi_j} \sim \frac{1}{\xi^4} \quad \text{(planar)}. \tag{6.18}$$

It is clear from (6.17) and (6.18) that the nonlinear terms are small compared with all other terms at large radii.

The limit $\xi \to 0$ requires some care owing to the singular behaviour of the velocity field for cases with $k \geqslant \frac{1}{2}$. The planar case is of particular interest because of the logarithmic singularity at the origin. For small ξ we have the following estimates using asymptotic forms of the axisymmetric solutions given above:

$k = \frac{1}{4}$

$$U_i \sim C_1 + C_2 \xi^2; \quad P = 0; \quad \frac{\partial}{\partial \xi_j}(U_i U_j) \sim Re^2 \xi; \quad \frac{\partial^2 U_i}{\partial \xi_j \partial \xi_j} \sim C_2 + C_3 \xi^2; \tag{6.19}$$

$k = \frac{1}{2}, \frac{3}{4}$

$$U_i \sim \frac{C_1}{\xi}; \quad \frac{\partial P}{\partial \xi_i} \sim \frac{1}{\xi^3}; \quad \frac{\partial}{\partial \xi_j}(U_i U_j) \sim Re^2\left(\frac{1}{\xi^3}\right); \quad \frac{\partial^3 U_i}{\partial \xi_j \partial \xi_j} \sim \left(\frac{1}{\xi^3}\right). \tag{6.20}$$

In the case of the vortex ring ($k = \frac{1}{4}$) the Stokes approximation is uniformly valid over the full range $0 \leqslant \xi < \infty$. In fact, in the neighbourhood of the origin the convective terms are small compared with the rest at all Reynolds numbers. This leads one to expect that the Stokes solution should be the appropriate $\xi \to 0$ limit for the nonlinear problem in this case. Note that for the vortex ring and vortex pair ($k = \frac{1}{4}, \frac{1}{3}$) the pressure is zero for $t > 0$ since for these cases the time rate of change of the impulse is zero. In the case of the round jet ($k = \frac{1}{2}$) the Stokes approximation is also uniformly valid over $0 \leqslant \xi < \infty$. This is not obvious since the ratio of nonlinear convective to acceleration terms appears to be $\sim Re^2/\xi^2$ which for small but finite Re will diverge as $\xi \to 0$. However in this case the small-ξ limit is a steady flow and the

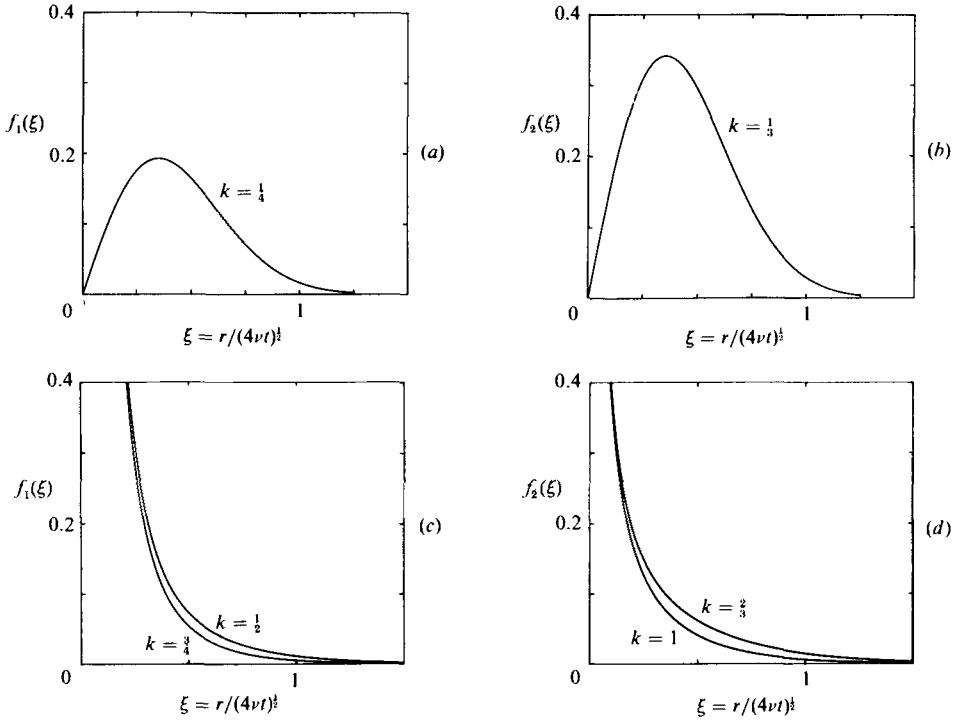

FIGURE 4. Radial vorticity distributions, $f_1(\xi)$, $f_2(\xi)$ for (*a*) the vortex ring ($k = \frac{1}{4}$), (*b*) the vortex pair ($k = \frac{1}{3}$), (*c*) the round jet and ramp jet ($k = \frac{1}{2}, \frac{3}{4}$), (*d*) the plane jet and plane ramp jet ($k = \frac{2}{3}, 1$).

acceleration term is identically zero. The appropriate comparison in this limit is only between pressure-gradient, viscous and convective terms for which the ratio is $\sim Re^2$. For the case of the ramp jet ($k = \frac{3}{4}$) the region near the origin is essentially non-steady and the comparison of convective to non-steady terms has to be retained. The unsteady Stokes approximation in this case appears to lose validity inside a radius such that $Re^2/\xi^2 \sim O(1)$. In physical coordinates this is a growing circle of radius $r \sim t$.

For the planar cases the estimates of various terms are

$k = \frac{1}{3}$

$$U_i \sim C_1 + C_2\xi^2; \quad P = 0; \quad \frac{\partial}{\partial \xi_j}(U_i U_j) \sim Re^{\frac{3}{2}}\xi; \quad \frac{\partial^2 U_i}{\partial \xi_j \partial \xi_j} \sim C_2 + C_3\xi^2; \tag{6.21}$$

$k = \frac{2}{3}, 1$

$$U_i \sim \ln \xi; \quad \frac{\partial P}{\partial \xi} \sim \frac{1}{\xi^2}; \quad \frac{\partial}{\partial \xi_j} U_i U_j \sim Re^{\frac{3}{2}} \frac{\ln \xi}{\xi^2}; \quad \frac{\partial^2 U_i}{\partial \xi_j \partial \xi_j} \sim \frac{1}{\xi^2}. \tag{6.22}$$

As for the vortex ring, the Stokes approximation to the vortex pair ($k = \frac{1}{3}$) is uniformly valid over $0 \leqslant \xi < \infty$ with the validity near $\xi = 0$ holding for all Reynolds numbers. The plane-ramp-jet ($k = 1$) Stokes approximation is valid in the range outside a circle of radius such that $Re^{\frac{3}{2}}/\xi^2 \sim O(1)$. Inside the circle the convective terms dominate the acceleration terms as $\xi \to 0$. The pressure-gradient and viscous terms dominate the convective terms throughout $0 \leqslant \xi < \infty$. The case of the plane jet ($k = \frac{2}{3}$) requires closer study. As for the round jet, the ratio of convective to acceleration terms diverges as $\xi \to 0$ and the Stokes approximation would appear to

become invalid. However, in contrast to the round jet, the stream function and velocity for the plane-jet solution are essentially unsteady. In this limit

$$\left.\begin{aligned} A_z &= M(4\nu)^{-\frac{1}{2}} t^{\frac{1}{2}} \left(\frac{\sin\theta}{4\pi}\right) \{-\xi \ln(\xi) + \tfrac{1}{2}(1-\gamma)\,\xi + \tfrac{1}{4}\xi^3\}, \\ u &= M(4\nu)^{-1} \left(\frac{\cos\theta}{4\pi}\right) \{-\ln(\xi) + \tfrac{1}{2}(1-\gamma) + \tfrac{1}{4}\xi^2\}, \\ v &= M(4\nu)^{-1} \left(\frac{\sin\theta}{4\pi}\right) \{\tfrac{1}{2}\ln(\xi) + \tfrac{1}{2}(1+\gamma) - \tfrac{3}{4}\xi^2\}, \\ \omega &= M(4\nu)^{-\frac{3}{2}} t^{-\frac{1}{2}} \left(\frac{\sin\theta}{4\pi}\right) \left\{-\frac{1}{\xi} - \tfrac{1}{2}\xi + \tfrac{1}{4}\xi^3\right\}. \end{aligned}\right\} \tag{6.23}$$

The quantities A_z, u, and v all depend on $\ln(4\nu t)$ in the limit $\xi \to 0$. However the vorticity is independent of time:

$$\frac{\partial \ln \xi}{\partial r} \sim \frac{1}{r} \Rightarrow \lim_{\xi \to 0} \omega_z = M\nu^{-1} \frac{\sin\theta}{4\pi r}. \tag{6.24}$$

Estimates of the convective and diffusive terms in the vorticity equation give, near $\xi = 0$,

$$U \frac{\partial W}{\partial \xi} \sim Re^{\frac{3}{2}} \frac{\ln \xi}{\xi^2}; \quad \frac{\partial^2 W}{\partial \xi^2} \sim \frac{1}{\xi^3}. \tag{6.25}$$

Diffusion of vorticity dominates convection over the full range $0 \leqslant \xi < \infty$.

A comment on Stokes' paradox

The plane-jet solution (6.12) and its limiting behaviour (6.23) provide some insight into the problem of constructing low-Reynolds-number approximations to planar flows. In general planar solutions of the biharmonic equation for the stream function contain logarithmic terms which lead to infinite velocities at large radius. The classic case is the linear solution for steady flow around a circular cylinder worked out by Stokes in 1851. The singular behaviour of the logarithmic term prevents the solution from being able to match uniform flow conditions at infinity. The breakdown of the Stokes approximation is usually attributed to the fact that there will always be a region where the ratio of convective to diffusive terms $\sim rRe$ will be of order one regardless of the magnitude of Re (Van Dyke 1975). A solution to the so-called Stokes paradox was provided by Oseen (1910) who added a linear convective term to the Stokes equations. Although this approach was *ad hoc* in nature it did provide a uniformly valid solution to the problem and computations of the full equations generally follow Oseen's solution at low Reynolds number.

Stokes regarded the paradox as an indication that no steady flow exists. Any real flow has to be started from rest. The complete solution therefore must include the starting process and one can reason that the large-time limit might retain a residue of the initial transient. Although Stokes' argument seems to have been discounted in connection with the cylinder problem, it remains central to the case of the plane jet where the Oseen correction is not available. In this case the inclusion of the starting process is essential and leads directly to the solution (6.12) which contains logarithmic terms but in a benign form multiplied by a decaying exponential. The exponentially decaying vorticity at infinity associated with the start-up ensures an algebraically decaying velocity field and an overall solution which, though only valid

for small time, is uniformly valid over all space. Although the fact that, at small radius, the Stokes approximation is apparently valid for vorticity but not velocity might be regarded as paradoxical. The contrast with the impulsively started round jet is important. In this case a steady flow is established in the neighbourhood of the force at $t = 0^+$ and remains steady for all time. This is true for the low-Reynolds-number limit as well as the full nonlinear problem in which the limiting flow at $\xi \to 0$ corresponds to the classical exact Landau (1944)–Squire (1951) solution of the steady jet. In the case of an impulsively started plane jet a steady vorticity field is established at $t = 0^+$ but the velocity field and stream function remain logarithmically unsteady at least up to the time the Stokes limit becomes invalid. This occurs when

$$Mt^{\frac{1}{3}}/\nu \sim O(1). \tag{6.26}$$

Eventually a steady flow near $\xi = 0$ should be established but precisely when this occurs and whether only the next order, several orders or all orders of approximation in time will be required remains an open question.

6.2. *Critical Reynolds numbers*

As mentioned above, the self-similar tangential velocity $V(\xi, \theta)$ of the Stokes solution always has a zero at a fixed radius ξ_0 for all θ. From (4.11) we see that the critical Reynolds number Re_1 at which the on-axis node begins to bifurcate to a saddle and off-axis node occurs when

$$Re_1^{\frac{1}{2}m} = \frac{\xi_0}{2U(\xi_0, 0)}. \tag{6.27}$$

This expression is somewhat easier to evaluate for Re_1 than (5.32) which requires the construction of $q(Re)$. The second critical Reynolds number Re_2 at which the off-axis node begins to spiral is found using (5.33). This requires the construction of q but the procedure is simplified somewhat by the fact that $\xi_c = \xi_0$ for the off-axis critical point at all Reynolds numbers. When ξ_0 is substituted into (4.11) the result is a relationship between θ_c and Re:

$$Re_2^{\frac{1}{2}m} = \frac{\xi_0}{2U(\xi_0, \theta_c)}. \tag{6.28}$$

A further manipulation to form q leads to a unique specification of Re_2 through the condition given by (5.33). This is the basic procedure for finding the critical Reynolds numbers in all six Stokes flow solutions. The resulting values of ξ_0, Re_1 and Re_2 are given in table 1. Note that the critical Reynolds numbers are quite low compared with typical instability Reynolds numbers of free-shear flows and are likely to be even lower in the nonlinear case. The critical Reynolds numbers exhibit the same sort of trend as the root ξ_0. Both Re_1 and Re_2 decrease as k increases for a given m and the critical Reynolds numbers of the planar case tend to be lower than those of the axisymmetric case for a given n. All this is consistent with the notion that disturbances are stronger in two dimensions than in three. In the case of the numerical solution of the round jet the critical Reynolds numbers of the nonlinear problem were found to be lower than those deduced from the Stokes approximation (Cantwell & Allen 1984) which is consistent with the notion that nonlinearity is destabilizing.

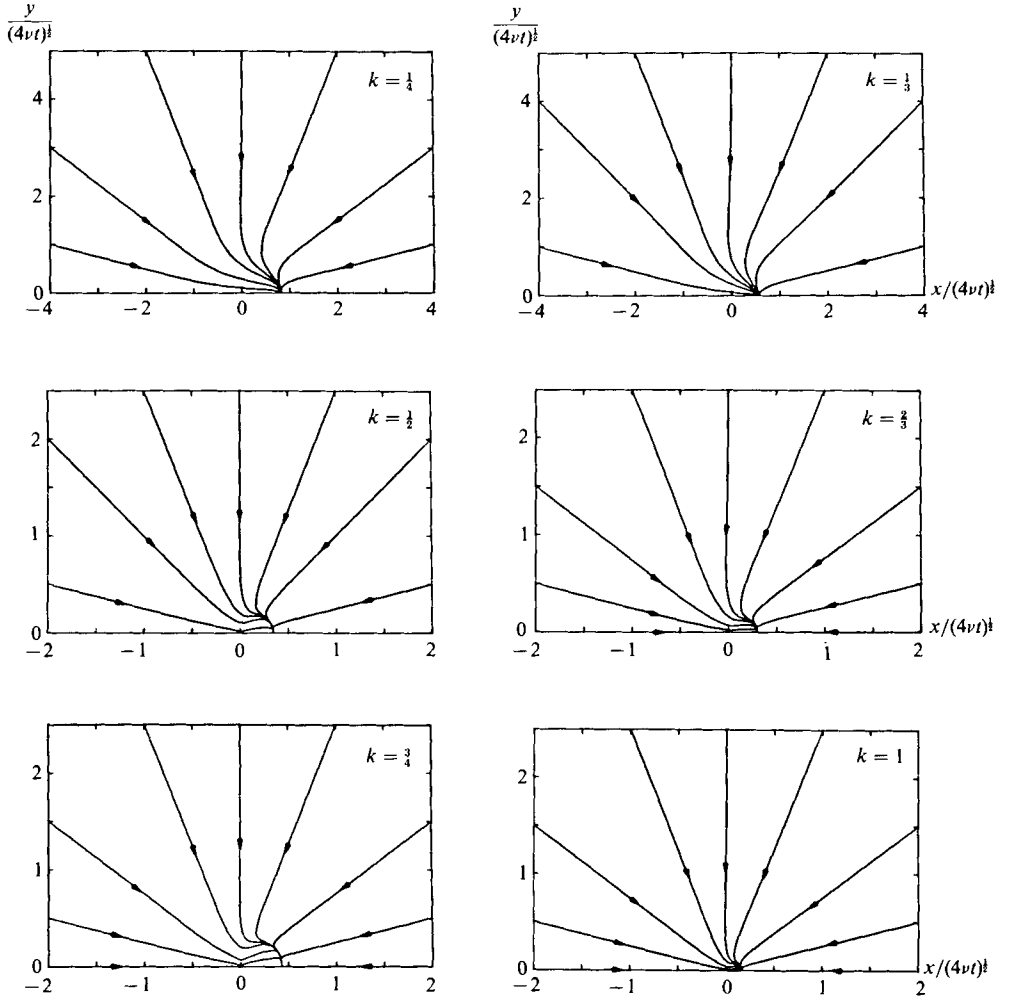

FIGURE 5. Entrainment diagrams for $Re < Re_1$.

7. Discussion

Entrainment diagrams for the various cases are given in figures 5, 6 and 7 corresponding to Reynolds-number ranges $Re < Re_1$, $Re_1 < Re < Re_2$ and $Re > Re_2$ respectively. These patterns are constructed by forward integration of (4.2) for a set of initial points arranged in a semicircle about the origin. The Reynolds number is held fixed during the integration so that the resulting trajectories depict the instantaneous vector field $(Re^{\frac{1}{2}m}\, U - \frac{1}{2}\xi,\ V/\xi)$. The vector field in these figures can be thought of as a flow in a contracting space of divergence -1 or $-\frac{3}{2}$ depending on the number of dimensions. It is a flow with a uniform distribution of sinks as it might be seen by an observer who is receding out of the plane of motion at a rate proportional to $1/t^{\frac{1}{2}}$. Fluid appears to vanish into the critical points but in fact there is no violation of continuity, there are no infinities at the critical points and changes in topology occur smoothly as the Reynolds number crosses critical values. Note the factor of 2 in the scale of the axes of the vortex ring and vortex pair compared with

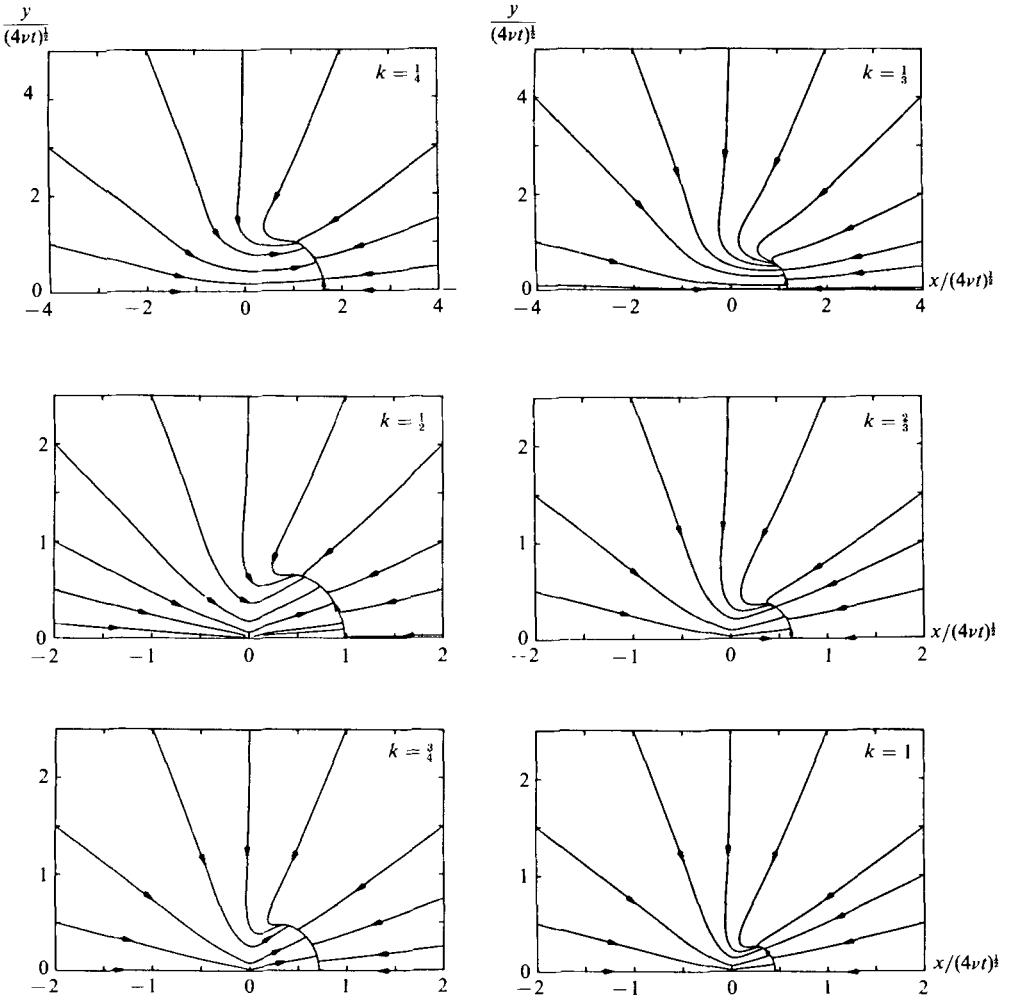

FIGURE 6. Entrainment diagrams for $Re_1 < Re < Re_2$.

the other four cases. To aid in the interpretation of these diagrams a cine film has been made which depicts the movement, in physical coordinates, of timelines subjected to the motion of the round jet, vortex ring and ramp jet. Several frames from this film are shown in figures 8 and 9. A copy of the film can be obtained on loan by request to the author.

All six cases exhibit the three basic states of motion shown schematically in figure 2(*c*). The entrainment diagrams for the lowest-Reynolds-number state, shown in figure 5, are dominated by the radial inflow induced by the scaling of coordinates. In the limit $Re \to 0$ the critical points would move to the origin and the entrainment diagrams for the vortex ring, vortex pair, plane jet and plane ramp jet ($k = \frac{1}{4}, \frac{1}{3}, \frac{2}{3}, 1$) would reduce to a simple star pattern converging to the origin while the trajectories of the round jet and ramp jet ($k = \frac{1}{2}, \frac{3}{4}$) would retain their nodal character. We deduced this result in §4.2 when we worked out the values of p and q for the $\xi \to 0$ limit of the various cases.

Figure 6 shows the entrainment diagrams for the intermediate-Reynolds-number

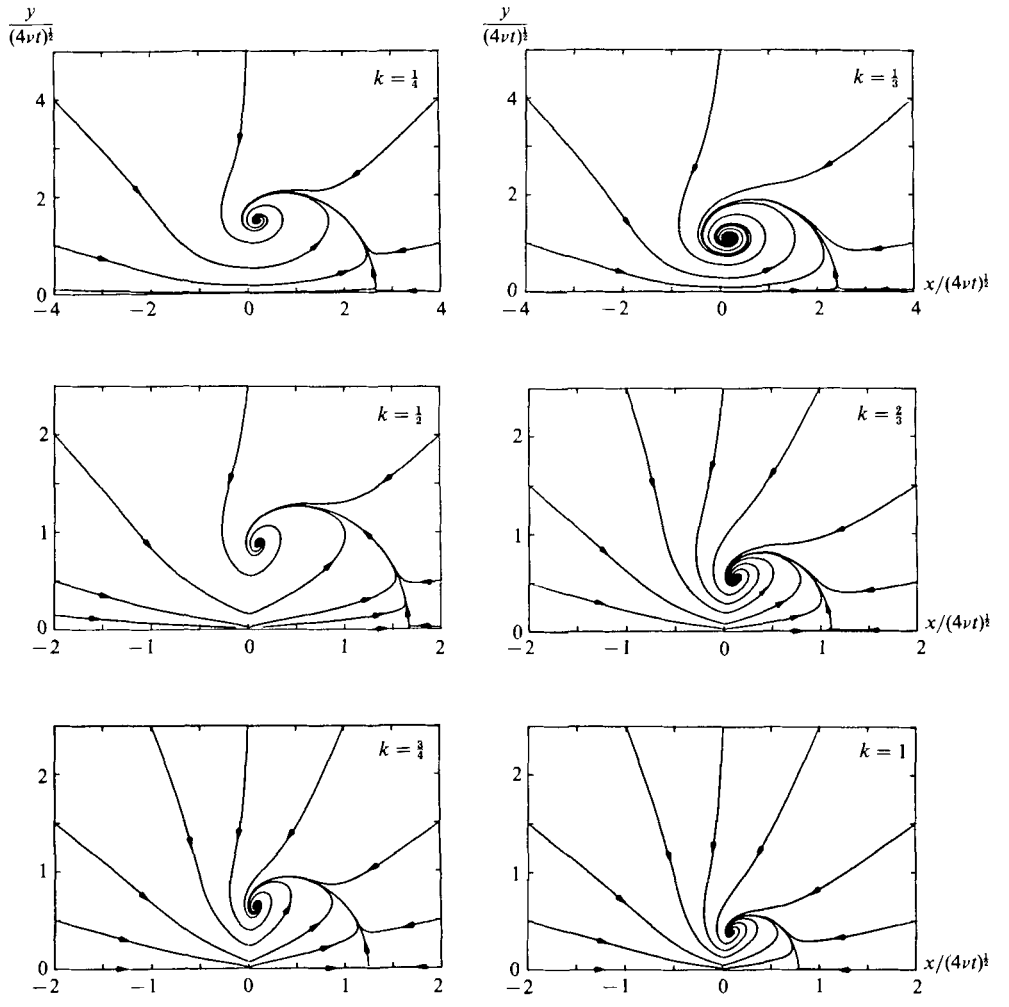

FIGURE 7. Entrainment diagrams for $Re > Re_2$.

state. The on-axis node has moved outward, changed to a saddle, and all trajectories converge to the off-axis stable node. At the scale of these diagrams the nodal point itself is quite difficult to resolve. The region over which the radial direction of the trajectories changes sign is very thin and gives the appearance of a nodal line emanating from the on-axis saddle. The convergence of trajectories into a thin sheet before they reach the critical point is also evident in the high-Reynolds-number state depicted in figure 7. There is an interesting variation with k in the shapes of the vortex roll-ups in figure 7. The non-singular cases of the vortex ring and, particularly, the vortex pair have broad well-defined foci with trajectories which spiral in at a shallow angle while the foci of the ramp jets are quite small and confined with trajectories which spiral in at a fairly steep angle. The angular position θ_c of the focal point increases with Reynolds number until it reaches $\frac{1}{2}\pi$ where it coincides with the point of maximum stream function. For the cases of the vortex ring and vortex pair the vorticity maximum of the Stokes solution is away from the critical point at all Reynolds numbers. This takes us back to the expressions for q in (4.22) and (4.23). The topology of the flow near the critical point is a consequence of the local balance

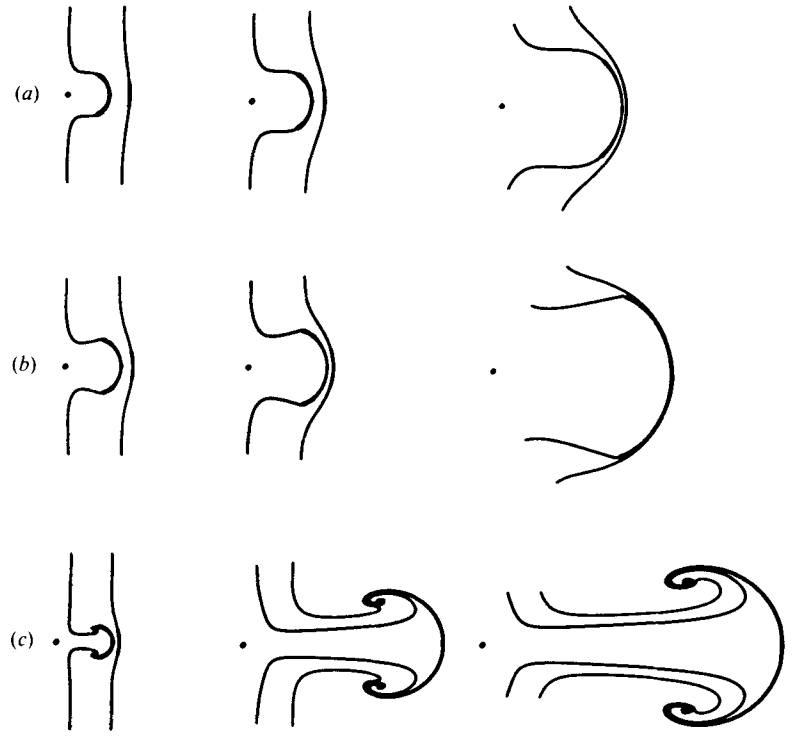

FIGURE 8. Distortion of timelines in physical coordinates under the action of the nonlinear round jet at (*a*) $Re = 4$, (*b*) $Re = 6$, (*c*) $Re = 30$. Time increases from left to right.

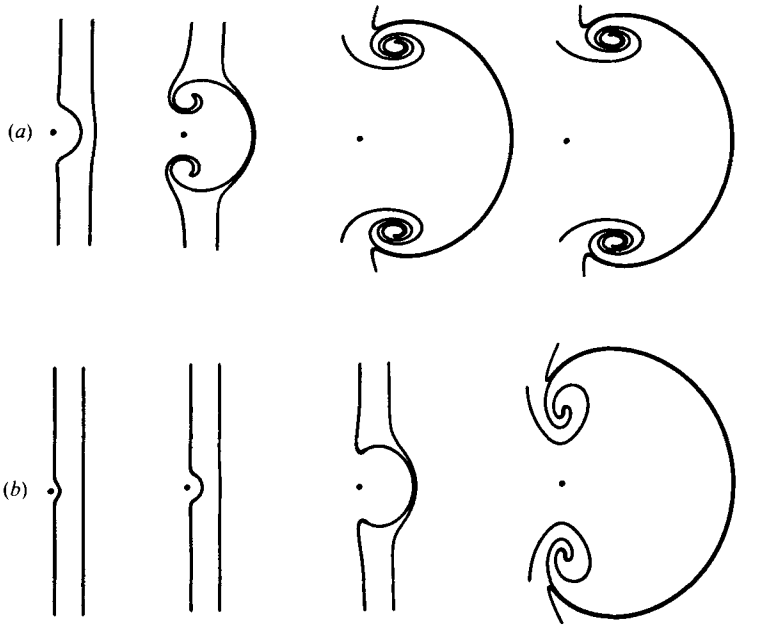

FIGURE 9. Distortion of timelines in physical coordinates under the action of (*a*) the Stokes vortex ring with initial Reynolds number equal to 100 and final Reynolds number much less than Re_1, and (*b*) the Stokes ramp jet with initial Reynolds number less than Re_1 and final Reynolds number equal to 30. Time increases from left to right.

between vorticity and strain and a focus does not in general correspond to a point of maximum local vorticity.

The time dependence of the Reynolds number in each case leads to contrasting physical interpretations of the respective entrainment diagrams. In the special case of the round jet the Reynolds number is independent of time and the trajectories represent true particle paths. Figure 8 shows several frames from the cine film which depicts the distortion of timelines under the motion of the round jet at Reynolds numbers in the three regimes of interest. The film was made from the numerical computations of the nonlinear problem reported in Cantwell & Allen (1984) although the basic motion of the Stokes solution is very similar. The main difference lies in the long slender stem and the small angle of spread in the nonlinear high-Reynolds-number case. The first critical Reynolds number defines the initiation of an intermediate state of motion between simple lateral straining concentrated on the jet axis, $Re < Re_1$. and vortex roll-up off the axis, $Re > Re_2$. Fluid lines which are initially smooth may form sharp corners as they are drawn into the region of the off-axis node (figure 8(*b*). The second critical Reynolds number defines the onset of a starting vortex. Perhaps the best experimental example of the flow depicted in figure 8(*c*) can be seen in G. I. Taylor's well-known film on low-Reynolds-number flow.

In the case of a vortex ring or vortex pair the entrainment diagram depicts the changing topology of the flow in the late stages of decay and Re_2 defines a dimensionless time at which the tendency of the flow to roll a fluid line terminates. The intermediate state $Re_1 < Re < Re_2$ occurs only briefly and sharp corners do not have time to form. One of the conclusions one can draw from this view of the decay of a vortex ring is that, if an initially straight timeline interacts with a vortex ring at a time that exceeds the critical time corresponding to Re_2, then no roll-up of this line will occur regardless of how long one waits and in spite of the fact that the streamline pattern is closed. This can be understood by observing that, in this case and in the case of the vortex pair, when $Re < Re_2$ the timing between the outward movement of the peak in the stream function and the convection of a given fluid line is such that no segment of the line has a chance to fully rotate before the centre in the streamline pattern has diffused away. Figure 9(*a*) shows several frames from the film which depicts this situation. Two initially vertical timelines are set into motion by the Stokes solution. The computation is carried out in physical coordinates and the initial Reynolds number is set at a value that greatly exceeds Re_2. As time proceeds the timeline closest to the origin rolls rapidly about the off-focus which, at this limiting Reynolds number, is centred on the peak in the stream function. The second timeline begins to roll but because it started life farther from the focus it does not complete a full rotation before Re_2 is reached. By the rightmost frame the motion is essentially dead and the second timeline will never be wrapped any further. Continued movement of the timelines as time increases is purely diffusive. On the axis, where the two timelines are subjected to a saddle-point motion, they merge and quickly become indistinguishable. The merging of timelines in all the cases depicted in figures 8(*b*, *c*) and 9 is a reflection of the behaviour suggested by the thinness of the region across which the radial direction of the trajectories in the entrainment diagrams of figures 6 and 7 changes sign.

Glezer (1981) investigated the turbulent vortex ring and found that the lengthscales of the ring varied as $t^{\frac{1}{4}}$, which is consistent with the notion that at high Reynolds number the large-scale structure is independent of ν. The entrainment diagram was shown experimentally to consist of two on-axis saddles rather than one, with the

second saddle behind the two foci. A similar structure appears in the case of the rising thermal studied by Griffiths (1986) although no second saddle appears in the computations of the round jet by Allen (1984). In the latter case the singularity at the origin produces a velocity field that decays monitonically with radius at all Reynolds numbers. Therefore there is only a single point at which the velocity and coordinate are in balance. In the non-singular cases of the vortex ring, vortex pair and thermal, the velocity field of the Stokes solution decays monitonically with radius but when the effects of nonlinearity are included the peak in the radial velocity convects in the direction of the force. This leads to a second point on the axis at which $Re^{\frac{1}{m}} U - \frac{1}{2}\xi = 0$, corresponding to the second saddle.

In the cases of the plane jet and two- and three-dimensional ramp jets the entrainment diagrams depict the early stages of the flow. As in the case of the vortex ring and vortex pair, the intermediate state $Re_1 < Re < Re_2$ occurs only briefly and smooth lines subjected to the motion will not develop corners. The second critical Reynolds number defines a dimensionless time at which a starting vortex begins. Because the Reynolds number increases with time any timeline will eventually be rolled into the off-axis focus. Figure 9(*b*) shows several frames from the film which depict this case. As time increases the rolled-up timeline becomes somewhat V-shaped. This is characteristic of all the cases with $k \geqslant \frac{1}{2}$ and is related to the interaction of the timeline with the singular velocity field near the origin. It is interesting to compare the shapes of the timelines in the neighbourhood of the centre of the roll-ups in figure 9(*a*) and (*b*). In the case of the vortex ring the timeline in this region is highly cusped, reflecting the early high-Reynolds-number history of the flow and the number of turns of the timeline is a measure of the magnitude of the initial Reynolds number. In the case of the ramp jet the timeline near the centre of the roll-up has a rather blunt nose, reflecting the slow distortion associated with the early low-Reynolds-number history of the flow. The outer timeline is nearly unmoved by the early motion but by the time the last frame of figure 9(*b*) is reached it has formed a cusp which will become more pronounced as the roll-up becomes more vigorous.

8. Concluding remarks

The mechanics of the starting process for a family of two- and three-dimensional jets has been studied in terms of particle trajectories of the Stokes solutions in a phase space of similarity coordinates. The vector field which results when the flow pattern is displayed in this manner provides a useful basis for comparison of various flow cases and a framework for understanding the role of the Reynolds number in determining flow behaviour. Six complementary cases are used to illustrate contrasting dependence on the Reynolds number. They all undergo a sequence of bifurcations in the topology of the phase portrait of particle paths as the Reynolds number is varied. Although the critical Reynolds numbers at which these bifurcations occur are quite low they exceed the range of validity of the Stokes approximation. However according to the analysis of the (p, q)-trajectory in §§4, 5 the nonlinear solution must follow the same sequence of topological states albeit with different, probably lower, critical Reynolds numbers.

The physical interpretation of the entrainment diagrams is straightforward in the case of the round jet for which the self-similar particle-path equations are strictly autonomous and the integrated trajectories are true particle paths. In this case a the non-autonomous cases the physical interpretation of the entrainment diagrams is not so straightforward. In these cases the forcing generates a flow which passes

through all three states of motion and the order in which the states are encountered depends on whether the Reynolds number is directly or inversely proportional to time. Nevertheless a knowledge of the critical Reynolds numbers and underlying topology is still useful for understanding the history of the motion and the movement of timelines and for identifying trends as the type of forcing is varied.

The Stokes solutions considered in this paper can be regarded as the lowest mode of an eigenfunction expansion of the full nonlinear solution. In this respect the entrainment diagrams depict the behaviour of this mode as it would contribute to the full solution over the entire range of Reynolds numbers. It is of considerable interest therefore to study the properties of higher modes and their nonlinear interactions and to search for the possible occurrence of temporally chaotic solutions of the particle-path equations as the Reynolds number is increased. Given the constraints on the (p, q)-trajectory imposed by continuity it seems unlikely that chaotic particle paths will occur unless the restriction to axisymmetric or planar flow is removed. In this case the flow would be described by a three-dimensional phase space with critical points characterized by three invariants. One may speculate that changes in flow topology will still occur through a, perhaps infinite, sequence of bifurcations associated with a series of critical Reynolds numbers. The nature of this sequence and whether it is associated with the onset of chaotic behaviour is a subject for further study.

This work was supported by the NASA Ames Research Center under grant NCA 2-IR745-502. I would like to express thanks to Gary Allen Jr. who produced the cine film of the jets and vortex rings. I would also like to acknowledge travel funds provided by the National Science Foundation and a grant for visiting scholars provided by the University of Melbourne. Thanks to Professor A. E. Perry and Dr M. S. Chong for many useful discussions and for the use of computer and photographic resources used to make the figures and write the paper. Thanks especially to Sharon Stanaway for her timely help in preparing the figures. This work was carried out while the author was on sabbatical leave at the University of Melbourne, Victoria, Australia.

REFERENCES

Allen Jr., G. A. 1984 Transition and mixing in axisymmetric jets and vortex rings. Ph.D. thesis, Stanford University, Department of Aeronautics and Astronautics, and *SUDAAR* No. 541.

Cantwell, B. J. Coles, D. E. & Dimotakis, P. E. 1978 Structure and entrainment on the plane of symmetry of a turbulent spot. *J. Fluid Mech.* **87**, 641–672.

Cantwell, B. J. 1981*a* Transition in the axisymmetric jet. *J. Fluid Mech.* **104**, 369–386.

Cantwell, B. J. 1981*b* Organized motion in turbulent flow. *Ann. Rev. Fluid Mech.* **13**, 457–515.

Cantwell, B. J. & Allen Jr., G. A. 1984 Transition and mixing in impulsively started jets and vortex rings. In *Proc. IUTAM Symp. on Turbulence and Chaotic Phenomena in Fluids, Kyoto, Japan*, pp. 123–132.

Glezer, A. 1981 An experimental study of a turbulent vortex ring. Ph.D. thesis, Graduate Aeronautical Laboratories, California Institute of Technology.

Griffiths, R. W. 1986 Particle motions induced by spherical convective elements in Stokes flow. *J. Fluid Mech.* **166**, 139–159.

Jackson, J. D. 1977 *Classical Electrodynamics*, pp. 140–181. Wiley.

Lamb, H. 1932 *Hydrodynamics*, pp. 214–216. Dover.

Landau, L. 1944 A new exact solution of the Navier–Stokes equations. *C. R. Acad. Sci. Dokl.* **43**, 286–288.

LIGHTHILL, M. J. 1963 In *Laminar Boundary Layer* (ed. L. Rosenhead), pp. 48–88. Oxford University Press.

OSEEN, C. W. 1910 Über die Stokessche Formel und über die Verwandte Aufgabe in der Hydrodynamik. *Arkiv for Mathematik, Astronomi och Fysik.* **6**, No. 29.

OSWATITSCH, K. 1958 Die Ablösungsbedingung von Grenzschichten. In *Grenzschichtforschung* (ed. H. Goertler), pp. 357–367. Springer. Also in *K. Oswatitsch: Contributions to the Development of Gasdynamics – Selected Papers translated (to English) on the occasion of K. Oswatitsch's 70th Birthday* (ed. W. Schneider & M. Platzer), pp. 6–18. Braunschweig, Wiesbaden: Vieweg 1980.

PERRY, A. E. & FAIRLIE, B. D. 1974 Critical points in flow patterns. *Adv. Geophys.* **18**, 299–315.

PERRY, A. E., LIM, T. T. & CHONG, M. S. 1980 Instantaneous vector fields in coflowing jets and wakes. *J. Fluid Mech.* **101**, 243–256.

PERRY, A. E. & CHONG, M. S. 1987 Eddying motions and flow patterns. *Ann. Rev. Fluid Mech.* **19** (to appear).

SOZOU, C. 1979 Development of the flow field of a point force in an infinite fluid. *J. Fluid Mech.* **91**, 541–546.

SQUIRE, H. B. 1951 The round laminar jet. *Q. J. Mech. Appl. Maths* **4**, 321–329.

STOKES, G. G. 1851 On the effect of the internal friction of fluids on the motion of pendulums. *Proc. Camb. Phil. Soc.* **9**, 52–57.

TAYLOR, G. I. 1923 Stability of a viscous liquid contained between two rotating cylinders. *Phil. Trans. R. Soc. Lond.* A **223**, 289–343.

TOBAK, M. & PEAKE, D. 1982 Topology of three-dimensional separated flows. *Ann. Rev. Fluid Mech.* **14**, 61–85.

TURNER, J. S. 1964 The flow into an expanding spherical vortex. *J. Fluid Mech.* **18**, 195–208.

VAN DYKE, M. 1975 *Perturbation Methods in Fluid Mechanics*, pp. 151–156. Parabolic.